Article

Optimization Design of Multi-Factor Combination for Power Generation from an Enhanced Geothermal System by Sensitivity Analysis and Orthogonal Test at Qiabuqia Geothermal Area

Yuan Zhao [1,2], Lingfeng Shu [1], Shunyi Chen [1], Jun Zhao [2] and Liangliang Guo [3,*]

[1] Powerchina HuaDong Engineering Corporation Limited, Hangzhou 311122, China;
zhao_y20@hdec.com (Y.Z.); shu_lf@hdec.com (L.S.); chen_sy@hdec.com (S.C.)

[2] Key Laboratory of Efficient Utilization of Low and Medium Grade Energy (Tianjin University), MOE,
Tianjin 300350, China; zhaojun@tju.edu.cn

[3] College of Water Resources Science and Engineering, Taiyuan University of Technology,
Taiyuan 030024, China

[*] Correspondence: guoliangliang@tyut.edu.cn

Abstract: In order to explore the optimal mining strategy of a fractured Enhanced Geothermal System (EGS) reservoir, we numerically investigated the influence of seven factors on heat production and conducted an optimization analysis of a multi-factor and multi-level combination by an orthogonal test based on the geological data at the Qiabuqia geothermal field. Seven factors were considered, including five reservoir factors (fracture spacing, fracture permeability, fracture permeability anisotropy, matrix permeability, and heat conductivity) and two operation factors (injected section length and injection rate). The results show that injection rate and fracture permeability have the greatest influence on production performance. Different factor combinations have a great influence on the productivity. The multi-factor and multi-level combination optimization is needed, and the optimization scheme of the EGS can be achieved through the orthogonal test and range analysis. The order of influence degree on the power generation is injection rate > fracture permeability > fracture permeability anisotropy > injected section length > matrix permeability > fracture spacing > heat conductivity. The order of influence degree on the coefficient of performance of the EGS is fracture permeability > injection rate > injected section length > fracture permeability anisotropy > matrix permeability > fracture spacing > heat conductivity. For reservoir stimulation, the stratum with dense natural fractures should be selected as the target EGS reservoir. It is not advisable to acidify the EGS reservoir too much to widen the apertures of the natural fractures. Fracture permeability anisotropy will increase pump energy consumption, but this adverse effect can be greatly reduced if the other parameters are well matched. Matrix permeability and heat conductivity may not be used as indicators in selecting a target reservoir. For project operation, the injected section length should be as long as possible. The injection rate plays a major role in all factors. Special attention should be paid to the value of the injection rate, which should not be too large. The appropriate injection temperature should be determined in accordance with the water source condition and the engineering requirement. If a commercial rate (100 kg/s) is to be obtained, the permeability of the reservoir fracture network needs to be stimulated to be higher. Meanwhile, in order to ensure that the production temperature is both high and stable, it is necessary to further increase the volume of the EGS reservoir.

Keywords: Enhanced Geothermal System; Hot Dry Rock; sensitivity analysis; orthogonal test; production performance

1. Introduction

In 2020, the Chinese government announced that China's carbon emissions would peak by 2030 and that China would strive to achieve carbon neutrality by 2060. Large-scale

non-carbon energy is urgently needed to improve China's energy structure. Geothermal energy is a competitive clean and renewable energy in coping with global climate change and emission reduction [1]. Hot Dry Rock (HDR) resources denote high temperature geothermal energy occurring in metamorphic or crystalline rock with low permeability and porosity. Its temperature ranges between 150 °C and 650 °C [1]. The first EGS project was prototyped at the Los Alamos National Laboratory at Fenton Hill in the 1970s, and subsequently, more than a dozen research and industrial projects have been carried out in various countries [1,2]. A systematic review of over 30 worldwide EGS projects can be found in Li et al. [2]. For the United States, the HDR resource reserve within a 3~10 km depth amounts to 14×10^6 EJ [1]. Located at the junction of three tectonic plates with a vast territory, China possesses abundant HDR geothermal energy. It is estimated that the HDR resource reserve within a 3~10 km depth in China's mainland amounts to 20.9×10^6 EJ, which is larger than that of the United States [3]. If 2% of the reserve was exploited, it would be equivalent to 4400 times China's total energy consumption in 2010 [3]. Since 2015, Chinese provincial governments have been actively investing in the exploration of HDR resources. Many potential HDR targets have been found, mainly including those in the Songliao Basin, southern Hainan, Wendeng, Datong, Zhangzhou, the Gonghe Basin, and the Subei Basin [4]. The Gonghe Basin is expected to be the first HDR pilot in China.

Although the HDR resource reserve is huge, it must be artificially stimulated to obtain economical geothermal fluids due to the low natural permeability of the reservoir. The technology integration for developing HDR energy is called the Enhanced Geothermal System (EGS) [1]. An EGS involves the creation of a fracture system in the target geological formation used for the injected geothermal fluid circulation. The geothermal structure of the target formation determines the upper limit of the HDR resource reserve. The characteristics of the target formation determine the property of the created EGS reservoir after stimulation. The operation conditions determine the amount of thermal energy actually extracted from the EGS subsurface system. Therefore, the scientific combination of the target reservoir factors and the operation factors has a great significance in the optimization of the EGS mining and in reducing the risks.

Hydraulic, chemical, and thermal stimulation techniques are currently available to stimulate existing fracture networks and/or create new fractures [2]. The cost of one reservoir treatment is approximately USD 0.5 M [4,5]. Multiple treatments can be more expensive. Numerical simulation has become an important research method for analyzing the production performance of EGS reservoirs. The numerical simulation needs to characterize and represent the subsurface fracture system. Natural fracture networks significantly control the hydrodynamic and thermodynamic behaviors in EGS reservoirs. The fracture–matrix interactions are treated with dual-continuum approaches, including equivalent porous media (EPM), the double-porosity method (DPM) [6], and the more rigorous multiple interacting continua (MINC) [7]. EPM is mainly used to model a densely fractured reservoir in which the fracture density is high and the fracture spacing is small; normally, the average fracture spacing is less than 2~3 m [8]. The DPM method is more reasonable when the average fracture spacing is higher than 10 m [8]. The MINC yields intermediate behaviors in between a porous medium and a single fracture. Suzuki et al. [9] conducted fractional diffusion modeling of heat transfer in porous and fractured media. They concluded that the porous model characterized the result of the MINC for the smaller fracture spacing (<5 m), while the single-fracture model agreed with the results of the MINC for larger fracture spacing (>20 m). In addition, the MINC method is able to describe gradients of pressures, temperatures, or concentrations inside the matrix by subdividing individual matrix blocks. It can be used to model the coupled hydrologic-thermal processes within the reservoirs. Fracture networks are the dominate channels for water to transfer mass and heat in an HDR reservoir. The discrete fracture network (DFN) model could simulate the fracture–matrix interactions based on the detailed fracture orientation, size, and spacing and other mechanical properties. Unfortunately, most of the measurement data are obtained from limited samples and do not accurately describe a fractured medium.

Parameter optimizations are the key to maximizing the heat extraction efficiency of the EGS. Many scholars have studied the conditions affecting the heat-production performance of the fractured EGS reservoir. Gong et al. [10] proposed a three-dimensional thermo-hydraulic model with multiple fracturing horizontal wells to evaluate the efficiency of the heat extraction in the EGS. Zhou et al. [11] studied the influence of randomly distributed fracture apertures in a fracture network on heat production from an EGS. Pandey et al. [12] researched the influence of fracture alteration on the heat production through the single-fracture THM model. The fractured EGS reservoir contains three porous media: rock matrix, natural fractures, and hydraulic fractures. Many EGS pilot production cases have revealed that the thermal reservoir is a highly heterogeneous fractured medium [13]. Compared to the fluid flow in a uniformly distributed porous medium, a fractured medium has an obvious preferential flow direction. Guo et al. [14] developed a 3D THM model with a 2D fracture layer to study the heterogeneity of the fractures on the heat-production efficiency and the service life of an EGS. Huang et al. [15] established an equivalent continuum 3D THM model to consider the heterogeneous permeability and porosity. Guo et al. [16] considered the THM coupled processes on the heterogeneity of fracture aperture and studied the influence of aperture heterogeneity on the flow behavior of fluid within a single-fracture system.

Although the numerical simulations of the EGS reservoirs have made great progress, there is still a lack of systematic study on the multi-factor combination conditions affecting the heat-production performance. These preliminary studies do not compare every condition and do not uncover the order of relative importance of the conditions affecting the heat production. Most productivity-optimization studies are focused on the effect of a single factor. Asai et al. [17] analyzed the effect of seven different flow schemes on the rate of heat production and obtained the optimum case when considering the rise in energy demand. Patterson et al. [18] optimized geothermal production in fractured rock reservoirs with a combination of simple analytical models, while considering reservoir structural uncertainty. Wu et al. [19] established a three-dimensional hydraulic fracturing model and used heat extraction as an evaluation indicator to optimize fracturing spacing and geothermal mining. Different reservoir factors and operation factors are involved in the optimization design of geothermal projects. Decision making in geothermal projects requires consideration of an optimal combination of different factors, rather than a single factor. There is little research on multi-factor combination analysis to optimize HDR productivity based on a comprehensive production index. The orthogonal test method is a kind of method to analyze the multi-factor and multi-level influence on system objectives and was proposed by Fisher in 1920 [20]. The orthogonal test method is a kind of approach that can compare every condition and rank in the order of relative importance of every condition. This method has been widely used in test design in science, engineering, and business [21,22]. Xie and Wang [23] conducted a performance optimization of a pinnate horizontal well in geothermal energy utilization with an orthogonal test. Yu et al. [24] proposed a modified zipper fracturing in an EGS reservoir and analyzed heat extraction optimization via an orthogonal test.

EGS projects are expensive and risky. All the factors of the project should be optimized as much as possible before operation. This makes engineering sense when improving production performance, reducing investment, and maintaining longer reservoir life. In this paper, the primary objective is to answer the following questions. (1) Which factors have the greatest impact on the productivity of an EGS reservoir? (2) How do these factors affect productivity over a long time, given that the EGS project is expected to serve for decades? (3) The EGS operation involves many factors and needs to meet several production indicators. The effect of different factors on the indicators may be the opposite. How can the combination of multi-factors be optimized to make all the indicators reach the best level? (4) Which factors should be considered in target reservoir selection and stimulation? In order to answer the above questions and explore the optimal mining strategy of a fractured EGS reservoir, we numerically investigated the influence of seven single factors

on heat production and conducted an optimization analysis of multi-factor and multi-level combinations by orthogonal test based on the geological data at the Qiabuqia geothermal field. The seven factors include five reservoir factors (fracture spacing, fracture permeability, fracture permeability anisotropy, matrix permeability, and heat conductivity) and two operation factors (injected section length and injection rate). The results could provide a scientific guidance for future fracturing design and reservoir operation at the Qiabuqia geothermal field.

2. Methodology

In this study, the geological and geothermal characteristics of the study area are studied first. Then, a three-dimensional hydraulic-thermal coupled numerical model is established for the fractured EGS reservoir using the MINC method. Adopting the selected reservoir factors and operation factors, the sensitivity of a single factor to the EGS productivity is analyzed by using a control variable method. According to the results of a single-factor sensitivity analysis, the most influential factors are screened out. Subsequently, the effects of a multi-factor and multi-level combination on EGS productivity are analyzed. Through the orthogonal test and range analysis, the order of influence degree of each factor on each performance indicator is determined. Finally, we conclude the optimal multi-factor and multi-level combination for EGS mining at the Qiabuqia area. The methodological flowchart is illustrated in Figure 1.
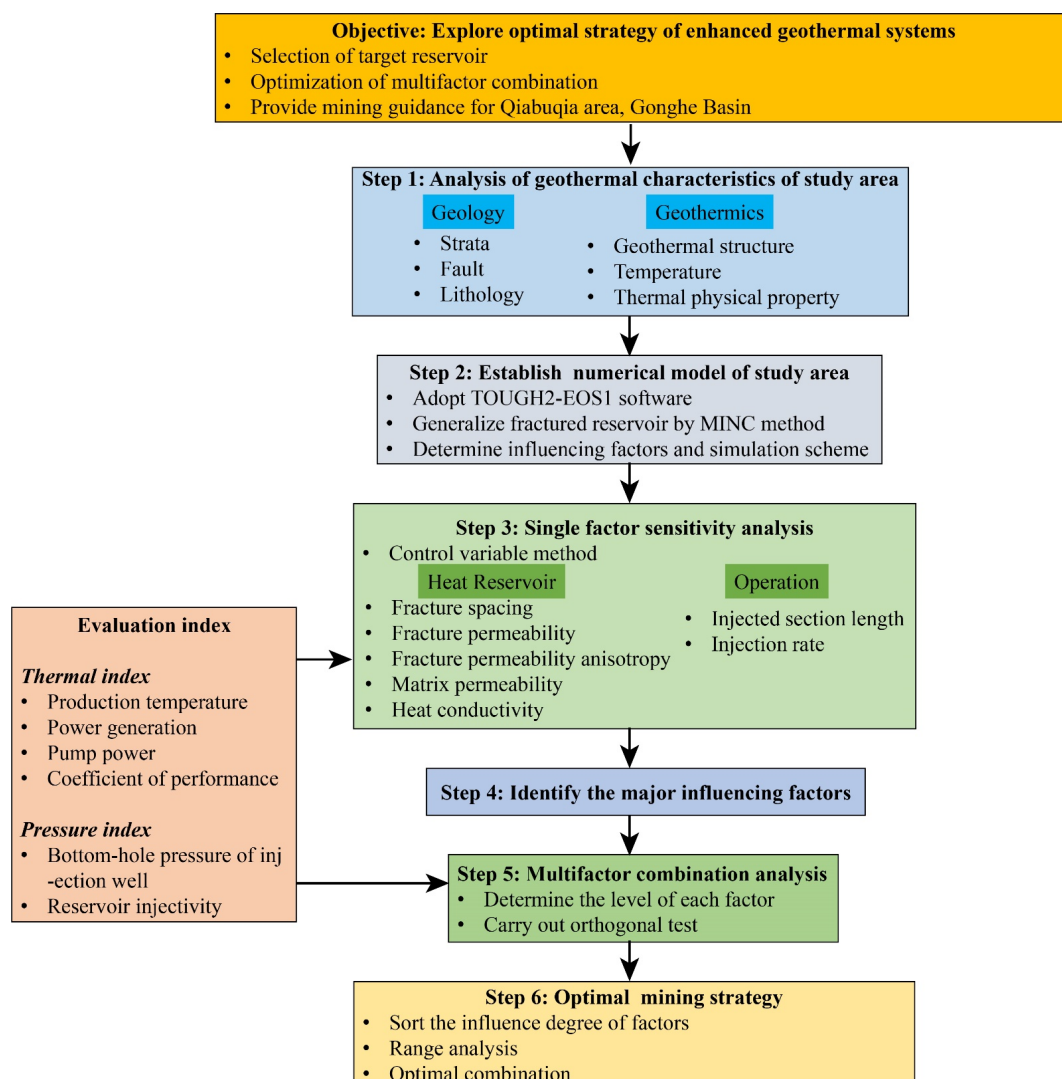

Figure 1. Methodological flowchart.

2.1. Governing Equation of Hydraulic-Thermal Coupled Numerical Model

TOUGH2 software was adopted for numerical simulation in this study. It is a well-accepted numerical simulation program for the multi-dimensional fluid and heat flows of multiphase, multicomponent fluid mixtures in porous and fractured media. The TOUGH2-EOS1 codes use the integral finite difference method to solve the conservation equations of mass, momentum, and energy, and their accuracy and reliability have been widely proven [8,9,25,26]. The theoretical background of the software is provided by [25]. In this study, water is used as the working fluid through the EGS reservoir. The mass–energy balance equation during the simulation can be written as:

$$\frac{d}{dt}\int_{V_n} M^{\kappa} dV_n = \int_{\Gamma_n} F^{\kappa} \cdot \vec{n} d\Gamma_n + \int_{V_n} q^{\kappa} dV_n,$$ (1)

where the quantity M represents mass or energy per volume; t is time; κ denotes mass components; V_n is an arbitrary subdomain of the flow system; F denotes mass or heat flux; q denotes sinks and sources; and n is a normal vector on surface element $d\Gamma_n$, pointing inward into V_n.

The mass accumulation term is:

$$M^{\kappa} = \varphi \Sigma S_{\beta} \rho_{\beta} X_{\beta}^{\kappa},$$ (2)

where φ denotes the porosity of the rock; S_{β} is the saturation of phase β (i.e., the fraction of the pore volume occupied by phase β); ρ_{β} is the density of phase β; and X_{β}^{κ} is the mass fraction of component κ present in phase β.

The heat accumulation term is:

$$M^{NK+1} = (1 - \varphi)\rho_R C_R T + \varphi \Sigma_{\beta} S_{\beta} \rho_{\beta} u_{\beta},$$ (3)

where ρ_R and C_R are, respectively, the density and specific heat of the rock; T is the temperature of the rock; and u_{β} represents specific internal energy in phase β.

The mass flux is given by:

$$F^{\kappa} = \Sigma_{\beta} X_{\beta}^{\kappa} F_{\beta},$$ (4)

The heat flux is calculated by:

$$F^{NK+1} = -\lambda \nabla T + \Sigma_{\beta} h_{\beta} F_{\beta},$$ (5)

where λ is the thermal conductivity and h_{β} is the specific enthalpy in phase β.

The governing equation of the β-phase Darcy flow in a fractured reservoir is:

$$F_{\beta} = \rho_{\beta} v_{\beta} = -k \frac{k_{r\beta}\rho_{\beta}}{\mu_{\beta}}\left(\nabla P_{\beta} - \rho_{\beta}g\right),$$ (6)

where v_{β} is the Darcy velocity (volume flux) in phase β; k is the absolute permeability; $k_{r\beta}$ is the permeability relative to phase β; and μ_{β} denotes the dynamic coefficient of viscosity.

2.2. Orthogonal Test Method

For the analysis of multi-factor and multi-level combinations, the orthogonal test method can represent complete tests through very limited combination tests and greatly reduces the workload [20–22]. It considers the characteristics of uniform dispersion and uniform comparability. Taking 3 factors (A, B, C) and 3 levels as an example, each factor has 3 levels ($a1$, $a2$, $a3$), ($b1$, $b2$, $b3$) and ($c1$, $c2$, $c3$), as shown in Table 1.

Table 1. Orthogonal test with 3 factors and 3 levels.

Level	Factor		
	A	B	C
Level 1	a1	b1	c1
Level 2	a2	b2	c2
Level 3	a3	b3	c3

A complete test would conduct $3 \times 3 \times 3 = 27$ trials in total, while only 9 trials are required according to the orthogonal test. The specific tests are listed in Table 2.

Table 2. Specific trials of orthogonal test for 3 factors and 3 levels.

Test Number	Factor		
	A	B	C
1	a1	b1	c1
2	a1	b2	c2
3	a1	b3	c3
4	a2	b1	c3
5	a2	b2	c1
6	a2	b3	c2
7	a3	b1	c2
8	a3	b2	c3
9	a3	b3	c1

2.3. Range Analysis

Based on the results of the orthogonal test, a range analysis is required to determine the relative importance of every factor and obtain the optimal combination [27]. The calculation formula of range, *R*, is

$$R = \max\{k_1, k_2, k_3, \ldots, k_n\} - \min\{k_1, k_2, k_3, \ldots, k_n\}, \tag{7}$$

$$k_i = \frac{K_i}{s}, \tag{8}$$

where *R* is range; K_i is the summation of the corresponding test results when the level number in each column is *i*; k_i is the average of K_i; and *s* is the sum of each level number in each column.

A larger *R* represents the greater importance of the factor. The optimal combination of factors and levels can be obtained according to the optimal *k* value of each factor.

3. Geothermal Characteristics of the Gonghe Basin

3.1. Geological Setting

The Gonghe Basin (GHB), located on the northeastern edge of the Qinghai-Tibet Plateau, is a rhombus-shaped intermountain basin extending to the NWW [28]. It is about 210 km long from east to west, 90 km wide from north to south, and has a total area of 21,186 km^2. It is the third largest basin in Qinghai Province, and the Yellow River runs across the short axis of the basin (Figure 2a). The GHB is a faulted basin formed since the Cenozoic. It is located at the intersection of the East Kunlun and West Qinling orogenic belts in the Qinling-Qilian-Kunlun fold system. It is bounded by the uplift of the fault fold belt. Affected by the fault activity on the boundary of the basin, the surrounding mountain ranges have been uplifting and rising recently, and the interior of the whole basin has relatively subsided. A set of huge Cenozoic sedimentary layers are formed in the basin, mainly composed of Quaternary alluvial deposits, river-lacust deposits, and Neo-Paleogene lacustrine deposits. The base of the basin mainly consists of intrusive rocks dominated by the Triassic strata and granite diorite (zircon dating from 222 to 245 Ma). The

Yanshan intrusive magmatic rocks (zircon dating from 180 to 195 Ma) are exposed on a small scale on the surface of the basin [26].
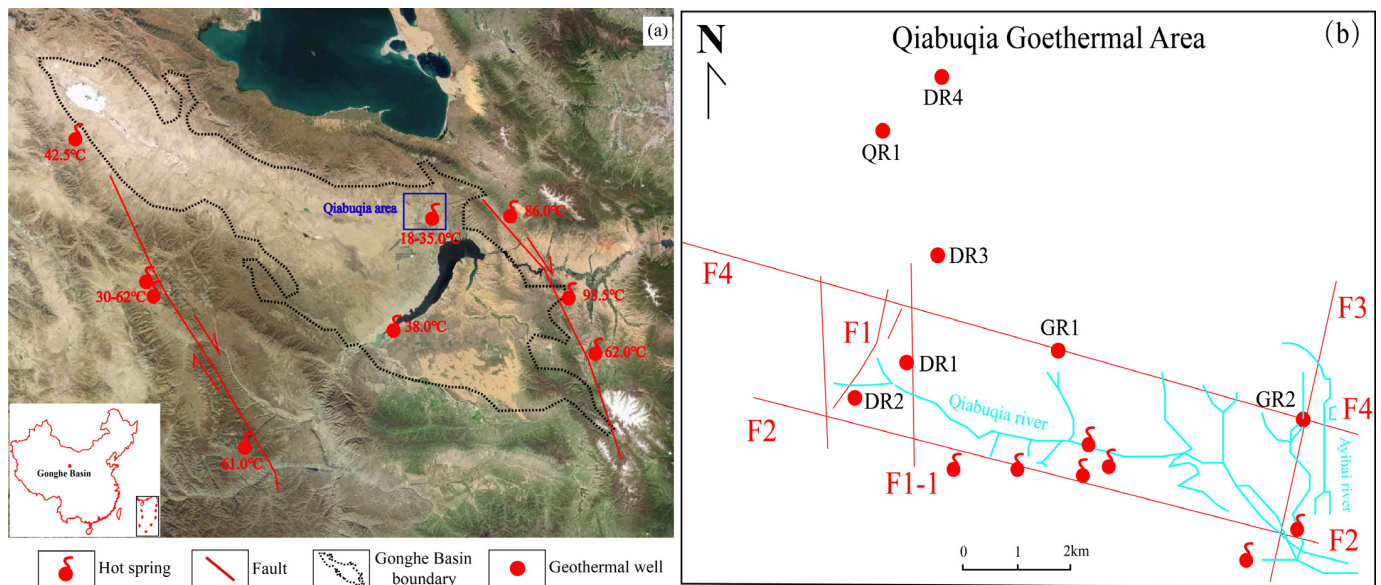
Figure 2. Location of Gonghe Basin (**a**). Distribution of geothermal wells and faults in the Qiabuqia area (**b**).

The Wahongshan fault in the western part of the basin is a right-lateral strike-slip fault zone with a strike of NNW. Three hot springs (42.5 °C, 30.0 °C~62.0 °C, and 61.0 °C) are exposed along the fault. In the east of the basin, there are also three hot springs on the front line of the right-lateral strike-slip fault zone of the Waligongshan Mountain, and the temperatures are 86.0 °C, 93.5 °C, and 62.0 °C, respectively [29].

The China Geological Survey selected the Qiabuqia geothermal area as the target HDR pilot. The geothermal abnormality in this area is obvious, and there are two groups of fault zones in the Neogene mudstone formation along the Shangtamai-Ayihai area. Both sets of fault zones cut through the base of the basin. Deep thermal energy surges up along the fracture zone (F2, F4), forming a high temperature abnormal zone (Figure 2b). There are seven geothermal wells in the Qiabuqia site, four of which are HDR exploration wells (DR3, DR4, GR1, and GR2) [28].

3.2. Geothermal Features

The terrestrial heat flow in the GHB is 65~78 mW/m^2, with an average of 72.58 mW/m^2, which is much higher than the average heat flow in mainland China (62.53 mW/m^2) [29]. It was reported from the DR3 and GR2 boreholes that the average heat flow is 119.3 mW/m^2. The core record of the GR1 hole shows that the strata of the basin can be divided into the following three parts (Figure 3):

(1) Part I (0~−505 m): The upper of Part I is a thin mid-late Pleistocene sand and gravel layer. Its grain gradually becomes finer downwards; the middle of Part I is mainly the lacustrine deposits of the Gonghe formation. The bottom of Part I is composed of sandy mudstone.

(2) Part II (−505~−1350 m): It is composed of the Linxia formation and the Xianshuihe formation. The lithology is mainly medium-thick mudstone and medium-thick siltstone. The integrity of the mudstone is better. The sandstone particles are finer.

(3) Part III (−1350~−3705 m): It is mid-late Triassic granite; the main lithology is granite and granodiorite. The radioactive heat generation rate of the granite ranges from 1.73 to 4.48 µW/m^3, with an average of 3.04 µW/m^3, and there is no abnormal high radioactive heat generation rate.
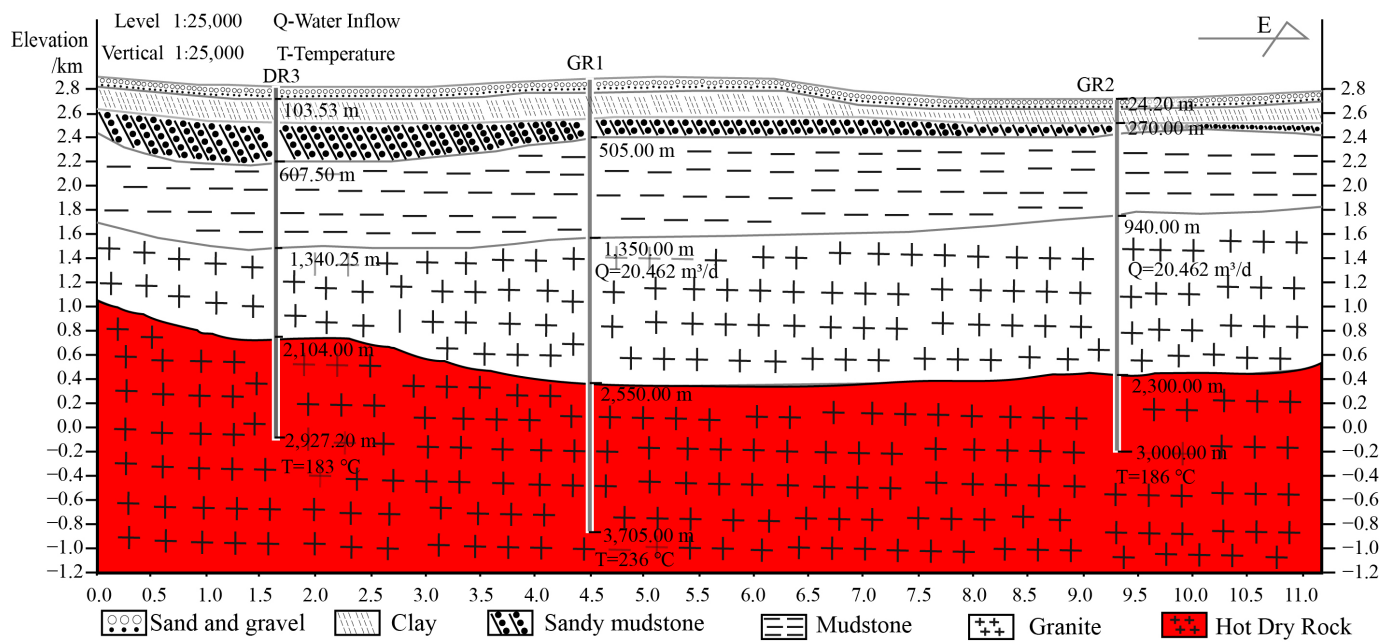
Figure 3. Geological section in the Qiabuqia area.

If the granite with a temperature greater than 150 °C is classified as HDR, the interface between the HDR and the overlying strata is shown in Figure 3. The HDR reservoir in the Qiabuqia area is located below about 2500 m.

Table 3 shows the temperature curves of four HDR exploration wells in the Qiabuqia area. The temperature data were measured using a DP-SJSW deep well thermometer. Within 0~−1500 m, the temperature gradients of GR1, GR2, DR3, and DR4 are 54.7, 46.7, 66.7, and 21.3 °C/km, respectively. Below −1500 m (to the bottom of each hole), the temperature gradients of GR1, GR2, DR3, and DR4 are 40.6, 50, 45, and 50.7 °C/km, respectively. The geothermal gradient in the HDR is 40.6~50.7 °C/km, and the formation temperature increases steadily with the depth, which belongs to the conductive geothermal energy [30]. The abnormal temperature of DR4 in the shallow part indicates that the basin is rich in hydrothermal resources in the shallow stratum (Part I and Part II).

Table 3. Measured temperature data of four geothermal wells.

Wells	Depth, z (km)	Measured Temperature, T (°C)
GR1	0.1~1.0	$T = 66.061z + 18.467$ ($R^2 = 0.9958$)
	1.1~2.8	$T = 40.289z + 48.992$ ($R^2 = 0.9967$)
	2.9~3.6	$T = 57.738z - 5.0238$ ($R^2 = 0.9861$)
GR2	0.1~3.0	$T = 50.154z + 33.795$ ($R^2 = 0.9996$)
DR3	0.1~1.4	$T = 72.879z + 14.198$ ($R^2 = 0.9988$)
	1.5~2.9	$T = 44.357z + 55.081$ ($R^2 = 0.996$)
DR4	0.1~0.5	$T = 7z + 77.3$ ($R^2 = 0.9423$)
	0.6~1.5	$T = 8.303z + 99.782$ ($R^2 = 0.91$)
	1.6~3.1	$T = 44.456z + 46.466$ ($R^2 = 0.9983$)

The geothermal structure includes heat sources, heat reservoirs, caps, and channels. Gao et al. [28] conducted magnetotelluric sounding interpretation and found that there may be a molten layer in the depth interval of 15~35 km. This molten layer may be the heat source for high-temperature geothermal resources in the GHB. The widely distributed huge-thick high-temperature granite formation is an ideal target reservoir for HDR. The cap rocks are mainly mudstone (Part II) and have the characteristics of low heat conductivity

(average 1.58 W/(m·K), Table 4). The thermal physical parameters were obtained by testing the core samples with a LFA447 laser thermal conductivity instrument in a laboratory. Therefore, it can effectively prevent the rapid loss of deep heat. The complex geological structure of the GHB has produced many deep, large faults, which can transfer the heat of the deep melt to the relatively shallow granite, thereby forming a relatively shallow high-temperature HDR reservoir [30].

Table 4. Heat conductivity of different lithologies with depth.

Lithology	Depth (km)	Heat Conductivity (W/(m·K))
Mudstone	0.20~1.40	1.25~1.99 (average is 1.58)
Igneous Rock	1.50–3.63	2.10–3.17 (average is 2.53)

4. EGS Reservoir Production Simulation Analysis

4.1. Target Reservoir and Project Design

The ideal target formation is one with a high temperature and well-developed natural fractures. Because reservoir stimulation has not been carried out in the study area, the geometry of the EGS reservoir is assumed in reference to the international EGS projects. The horizontal length of the Soultz EGS reservoir is about 2000 m, and the well spacing (GPK3-GPK2) is about 500 m [31]. The horizontal length of the Desert Peak EGS reservoir is about 2500 m, and the well spacing (27–15~22–22) is about 1000 m [32]. In this paper, the horizontal length of the created EGS reservoir in the Qiabuqia area is assumed to be 600 m, which is achievable according to current fracturing technology. Due to the subduction and compression of the Indian Ocean plate on the Eurasian continent, the internal horizontal tectonic stress in the GHB is relatively high. The dominant direction of the maximum compressive stress is in the NE direction, at about 51° [33]. It likely belongs to the stress mechanism of $\sigma_H > \sigma_V > \sigma_h$. Therefore, the stimulated EGS reservoir may be horizontal and may strip along the NE direction. Based on fracturing experience, the height and width of the created EGS reservoir are both assumed to be half its length, i.e., 300 m. Thus, the layer between the depths of 3700~4000 m is selected as the target reservoir, and the stimulated EGS reservoir geometry is assumed to be 600 m (length) × 300 m (width) × 300 m (height) (Figure 4). The natural fracture characteristics of the target reservoir are not clear; so, sensitivity studies are subsequently conducted to analyze the impact of the different fracture characteristics on productivity.

The vertical-doublet-well mode is the basis of another complex production mode. The injected section (L_{inj}) and the produced section (L_{pro}) are arranged diagonally, considering the buoyancy of the high-temperature fluid (Figure 4). The local surface water (i.e., river or lake) or groundwater is used as the injected water and makeup water. It is assumed that the injected water is heated to 10 °C when it reaches the injected section of the reservoir. After surface power generation and stepped heat exchange, the circulated water is reduced to 10 °C and then pumped back into the injection well. In order to study the variation of the heat transfer effect of the EGS during a long operation, the project lifetime is set to 50 years.

4.2. Power System

In designing a power generation system for the EGS project, a binary system utilizing an organic working fluid called ORC (Organic Rankine Cycle) technology was assumed to be the best choice. It is widely applied in EGS power plants [34,35]; thus, we also adopted it as the surface power generating system this time. Figure 4 shows the principle of operation of an ORC geothermal power plant. The working fluid receives energy from the geothermal fluid through a heat exchanger unit and evaporates; it then expands in the turbine, condenses, and is returned to the heat exchanger by a pump. The organic working medium should be selected according to the heat-source temperature. The temperature between the depths of 3700~4000 m in the Qiabuqia area is about 224 °C, which is similar

to that of the Soultz reservoir [31]. Therefore, isobutene was also adopted for the ORC system in Qiabuqia area.
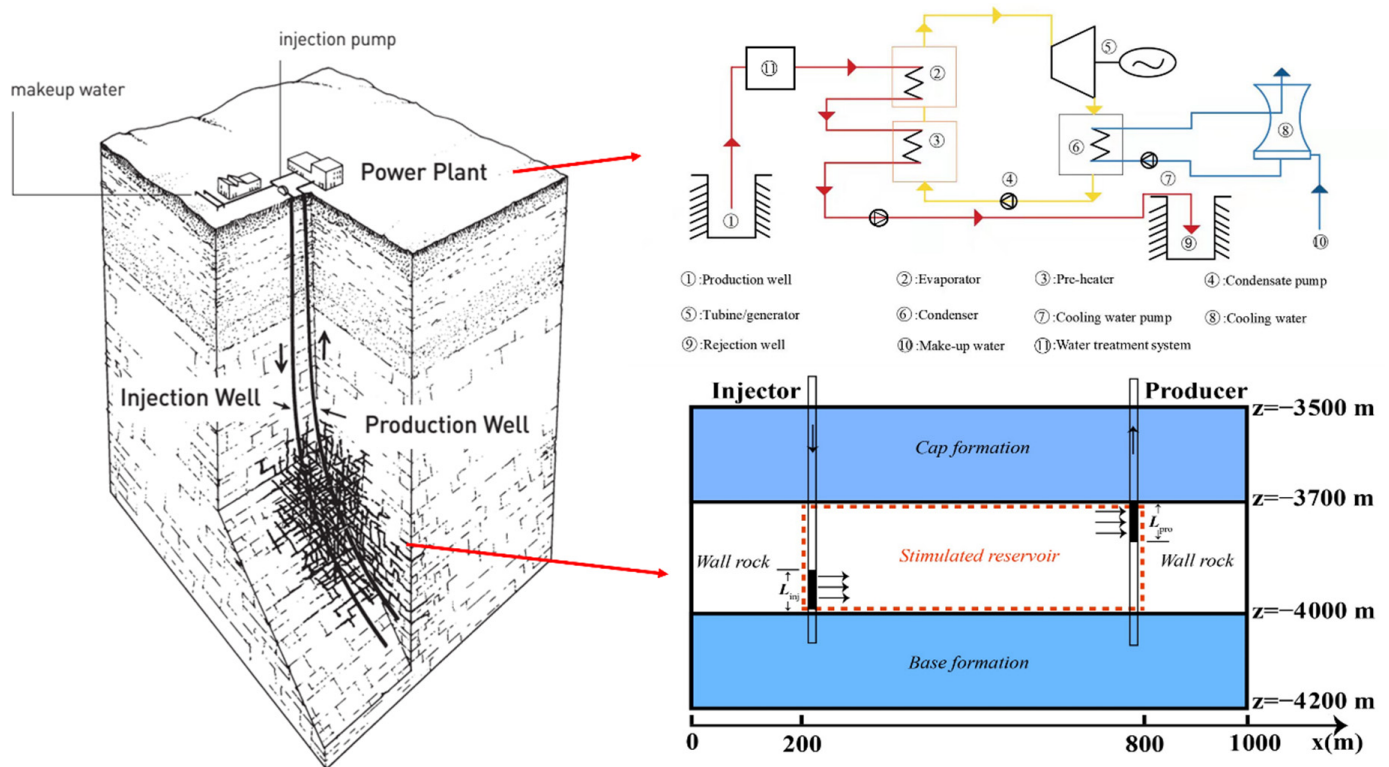

Figure 4. Schematic of EGS (**left**); operation diagram of surface ORC system (**right up**); conceptual model of stimulated EGS reservoir (**right down**).

4.3. Numerical Procedure

In this work, we used the TOUGH2-EOS1 code to simulate the thermal production performance of the EGS in the Qiabuqia area. The MINC approach was used to model the flow in the fractured EGS reservoir. It is a generalization of the classical double-porosity concept developed by Warren and Root [7]. In the typical use of the dual-porosity option, the communication throughout the model is through the fractures, and communication between the fractures and matrix is through the interporosity flow defined by nested elements. The matrix blocks are discretized into a sequence of nested volume elements, which are defined on the basis of distance from the fractures (Figure 5).

Figure 5 illustrates the 3D hydraulic-thermal coupled numerical model corresponding to the conceptual model of Figure 4. The geometric size of the model is 1000 m (x) $\times$ 700 m (y) $\times$ 700 m (z). The grid number is 24 (x) $\times$ 21 (y) $\times$ 16 (z), with a total of 8064 primary cells. In order to get reliable results, the grid was refined to 5 m $\times$ 5 m $\times$ 30 m near the wells to accommodate the high pressure and thermal gradients. The matrix blocks were divided into four subgrids with volume fractions of 0.08, 0.2, 0.35, and 0.35. The fracture domain occupied a volume fraction of 0.02. After this partition, there was a total of 40,320 subgrid blocks nested in the 8064 gridblocks. This mesh scheme was verified by grid sensitivity analysis to ensure adequate accuracy of the solutions.
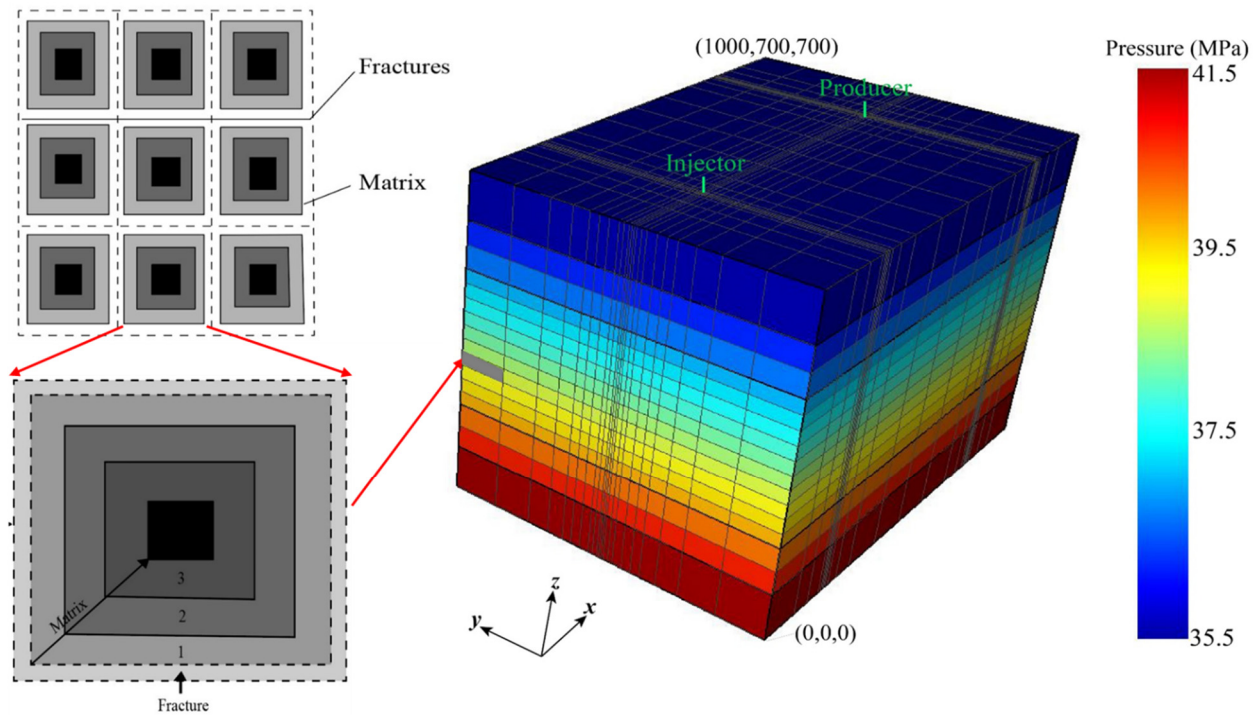
Figure 5. Subgridding in the MINC method (**left**) and the 3D numerical model (**right**).

4.4. Model Parameters and Single-Factor Sensitivity Scheme

Table 5 lists the values of the reservoir factors and the operation factors in the simulations. The matrix porosity, density, and specific heat are all based on the field data and laboratory experiments. A total of seven factors have been selected to study their influence on the thermal performance of the EGS. The factors consist of fracture spacing, fracture permeability, fracture permeability anisotropy, matrix permeability, heat conductivity, injected section length, and injection rate. We only changed one factor value in each simulation. The choice of factor is given as the following.

The larger the fracture spacing, the better the heat transfer effect of single fracture, but the tolerable total injection rate decreases for a certain length of injection section. In the Soultz project, the reservoir granite was pervasively fractured with a mean fracture spacing of about 3 m [31]. Therefore, the fracture spacing of the target reservoir was also assumed to 3 m in this paper and was selected as the base value for simulation. Meanwhile, a fracture spacing of 50 m was selected to represent a reservoir with sparse natural fractures. Suzuki et al. [9] concluded that the single-fracture model agreed with the results of the MINC for larger fracture spacing (>20 m). Thus, the MINC method is also suitable for a fracture spacing of 50 m.

The natural permeability of the deep granite in Qiabuqia is extremely low (about 1×10^{-16} m²~1×10^{-17} m²). After stimulation, the fracture permeability is generally increased by more than 1000 times [32]. In addition, through simulations, we found that when the fracture permeability was set as 1×10^{-14} m², the flow impedance of the reservoir still increased significantly (see Section 5.1). Therefore, the fracture permeability is assumed to be 1×10^{-13} m² as the base value. Through a long time of chemical stimulation, the fractures will be subjected to continuous corrosion, and the fracture permeability also increases. In order to evaluate whether excessive fracture permeability has a positive impact on productivity, we selected 1×10^{-11} m² for the simulation analysis.

As mentioned above, the horizontal tectonic stress in the GHB is relatively high, and an EGS reservoir dominated by horizontal fractures will likely be formed after fracturing. This will make the horizontal permeability of the reservoir larger than the vertical permeability [36]. Therefore, this paper considers the impact of fracture permeability anisotropy

on productivity. $\alpha = k_x/k_z = 10$ denotes that the fracture permeability in the z (vertical) direction is 10 times higher than that in the x (horizontal) direction.

Table 5. EGS reservoir properties and operation parameters.

Items	Parameters	Base Case Value	Selected Case Value
Reservoir	Fracture spacing, S_f	3 m	50 m
	Fracture permeability ($k_x = k_y = k_z$), P_f	1×10^{-13} m^2	1×10^{-11} m^2
	Fracture permeability anisotropy, α ($\alpha = k_x/k_z, k_x = k_y$),	1	10
	Matrix permeability, P_r	1×10^{-17} m^2	1×10^{-14} m^2
	Matrix porosity	0.025	No changed
	Matrix density	2360 kg/m^3	No changed
	Heat conductivity, λ_r	2.0 W/(m·K)	3.5 W/(m·K)
	Specific heat	754.4 J/(kg·K)	No changed
	Initial pressure	P = 4×10^{-7}–10,000z (Pa)	No changed
	Initial temperature	225 °C	No changed
Operation	Injected section length, L_{inj}	60 m	120 m
	Injection rate, q_{inj}	30 kg/s	20 kg/s
	Injection water temperature	10 °C	No changed
	Injection water specific enthalpy	78.77 kJ/kg	No changed
	Productivity index	5.4×10^{-12} m^3	No changed
	Production bottom-hole pressure	30 MPa	No changed

Matrix permeability is related to porosity; so, only the influence of matrix permeability on production is studied. The granite matrix is almost impermeable at about 1×10^{-17} m^2. However, some lithology may contain abundant micro-fractures or large dissolved pores, which may lead to higher permeability. Water would also flow through these pore spaces to extract heat [37]. Therefore, we studied the heat transfer effect under the condition of matrix permeability of 1×10^{-14} m^2.

According to Table 4, the heat conductivity of granite in the deep reservoir of Qiabuqia is between 2.10 W/(m·K) and 3.17 W/(m·K). In order to study the effect of heat conductivity on heat transfer, we slightly expanded the range, using 2.0 W/(m·K) as the base value and 3.5 W/(m·K) as the maximum value. In general, the heat conductivity of most crystalline rocks falls within this range.

In the EGS, both the injection sections and the pumping sections circulate water with the reservoir through casing perforations or grooves. Considering that this reservoir is only 300 m high in this study, the injected section lengths of 60 m and 120 m were chosen, respectively, for the simulations.

Injection rates are limited by temperature and pressure criteria. The simulations showed that 30 kg/s was the maximum injectable flow rate in this formation condition (see Section 4.6.1). For comparison, the effect of an injection rate of 20 kg/s on productivity was studied.

4.5. Initial and Boundary Conditions

In this study, all the boundaries were assumed to be no-flow for mass and heat transfer [4,8]. The wall rock, cap, and base layers were modeled thick enough to avoid boundary effects. The initial pressure conditions were assigned based on the hydrostatic pressure. As the height of the reservoir is only 300 m, the entire reservoir adopts a uniform temperature field. The initial reservoir temperature is 224 °C at a depth of 3850 m. For simplification, the fracture was assumed to be unchanged during the simulation process. Water losses were ignored, and the injection rate was assumed to be equal to the production rate.

4.6. Simulation Results of Single-Factor Sensitivity Analysis
4.6.1. Maximum Injection Rate under Base Case Condition

During the water circulation stage, when the cold water is injected into the stimulated reservoir, the reservoir pressure will grow and fluctuate with time. If the bottom-hole pressure of the injection well (P_{inj}) exceeds the reservoir minimum principal stress (σ_h),

the created fracture will dilate, giving rise to second reservoir growth and water losses; so, P_{inj} must be lower than σ_h. According to Ref. [33], the σ_h at a depth of 3700 m in the Qiabuqia area is about 66 MPa. Thus, the maximum injection rate can be determined by the pressure criterion:

$$P_{inj} < 66 \text{ MPa}, \tag{9}$$

The HDR resource development of Qiabuqia is mainly for electricity generation. If isobutene is chosen as the organic working medium, the production water temperature for the ORC generating electricity should meet the temperature criterion [38,39]:

$$T_{pro} > 105.36\,^{\circ}\text{C}, \tag{10}$$

where T_{pro} is the production water temperature.

Figure 6 shows the evolutions of T_{pro} and P_{inj} at different injection rates (q_{inj}) over the 50 years. When q_{inj} was 30 kg/s, the P_{inj} slightly increased from 37.92 MPa up to 38.38 MPa after 50 years of production. Meanwhile, T_{pro} decreased from 225 °C to a final 104 °C (down 53.8%). Within 50 years, the injection rate of 30 kg/s meets the pressure criterion and almost meets the temperature criterion. The injection pressure experienced three stages: slight rise, rapid rise, and slight rise. T_{pro} has gone through three stages: stable, rapid decline, and slight decline. When the injection rate became large, the water was pumped out before it fully exchanged heat with the reservoir, resulting in a rapid drop in the production temperature. When the heat-supplying reservoir from the wall rock is approximately equal to that taken away by water circulation, the production temperature tends to be stable again. From the 30th year to the 50th year, T_{pro} decreased by about 10 °C, while from the 45th year to the 50th year, T_{pro} decreased by only about 1 °C.

When q_{inj} is 80 kg/s, P_{inj} increases from the initial 38.62 MPa to 65.89 MPa in the 50th year. T_{pro} decreased from 225 °C to the final 31 °C. Within 50 years, the injection rate of 80 kg/s meets the pressure criterion but does not meet the temperature criterion. To ensure continuous power generation for the EGS, the maximum q_{inj} should be set to 30 kg/s.
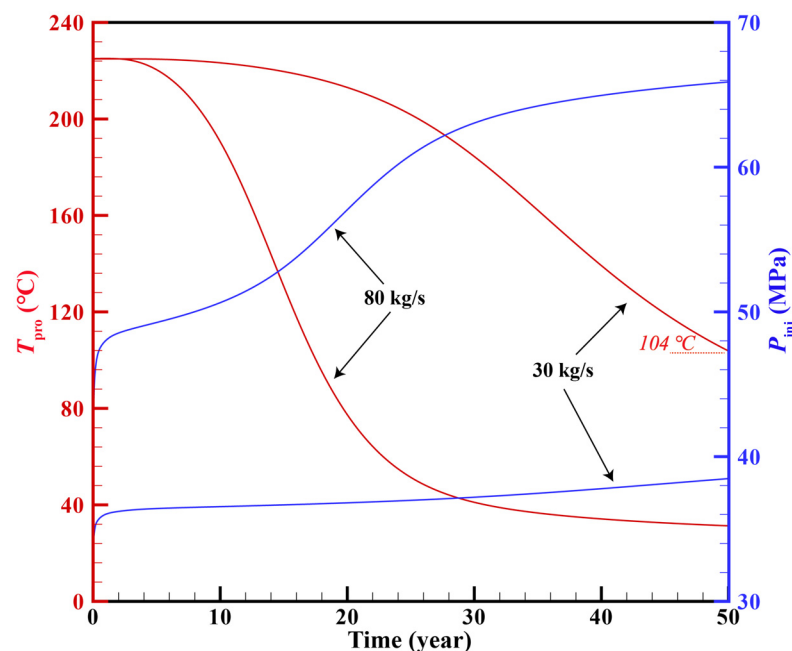
Figure 6. Evolutions of T_{pro} and P_{inj} at different injection rates (q_{inj}) over the 50 years.

4.6.2. Production Temperature

Figure 7 shows the evolutions of T_{pro} under different parameters over the 50 years. The curve of T_{pro} could be divided into two stages: the stable period and the decline period.

In the early stage of the EGS operation, the reservoir and wall rock contain sufficient heat; so, T_{pro} can be equal to the reservoir temperature. This stage belongs to the stable period. As cold water is continuously injected into the reservoir, the reservoir heat is continuously extracted. T_{pro} would enter decline period at some point. Among the seven selected parameters, P_f, α, and q_{inj} have the greatest influence on T_{pro}. The second is the S_f. While P_r, λ_r, and L_{inj} all have a slight effect on T_{pro}. The curve patterns of T_{pro} are in accordance with previous studies of Refs. [4,8,35].
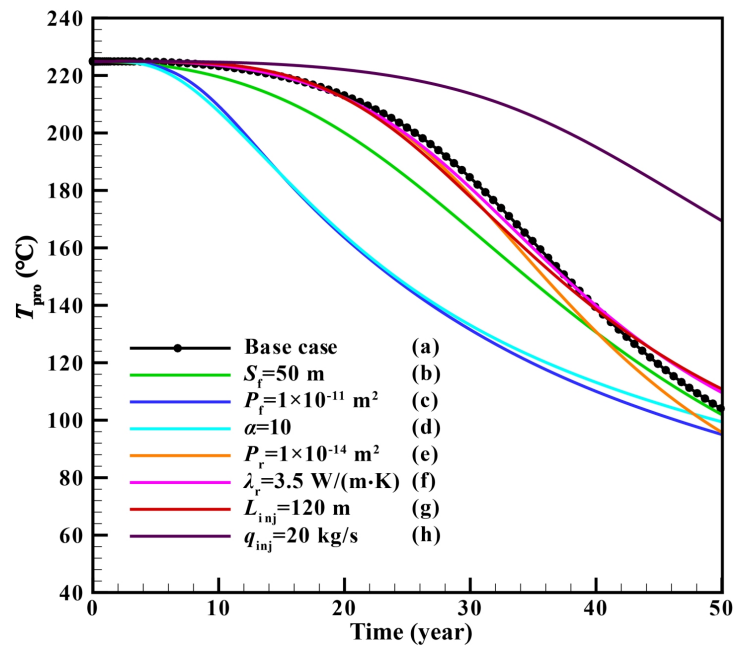

Figure 7. Evolutions of T_{pro} under different parameters over the 50 years.

4.6.3. Power Generation

Garg et al. derived a new expression for the available power generation, W_e, for the binary cycle with the following equation [38]:

$$W_e = \eta_e \frac{m_w(h_w - h_r)(T_R - T_P)}{(T_R - T_r)h_{sfgl}(T_b)} \left\{ \begin{array}{l} h_{sfgl}(T_b) - h_{sfl}(T_c) - T_{ck}\left[s_{sfg}(T_b) - s_{sfl}(T_c)\right] \\ -V_{sf}(T_C, P_{sfb})\left[P_{in} - P_{sfb}(T_c)\right] \end{array} \right\}, \quad (11)$$

where η_e, m_w, T, h, s, P, and V denote conversion efficiency, production rate, temperature, specific enthalpy, entropy, pressure, and specific volume, respectively. The subscripts w, r, R, P, b, c, g, l, in, sf, and k denote wellhead, reference, reservoir, pinch point, boiling, condenser, gas, liquid, inlet, secondary fluid, and Kelvin, respectively. More detailed descriptions of Equation (11) can be found in Ref. [40].

Figure 8 shows the evolutions of W_e under different parameters over the 50 years. The most influential factors are P_f, α, and q_{inj}. Comparing Figures 7 and 8, it can be seen that except for q_{inj}, the variation trends of W_e under the other six factors are the same as the trends of T_{pro}. Although T_{pro} declined much more slowly when q_{inj} decreased from 30 kg/s to 20 kg/s, the early W_e at 20 kg/s is lower than that at 30 kg/s due to the flow rate limitation. In the base case condition, the W_e in 50 years decreases from 2.53 MW to 0.16 MW, and the stable period is about 10 years. When q_{inj} is 20 kg/s, the W_e in 50 years is 1.69 MW~0.91 MW, and the stable period is about 13 years.
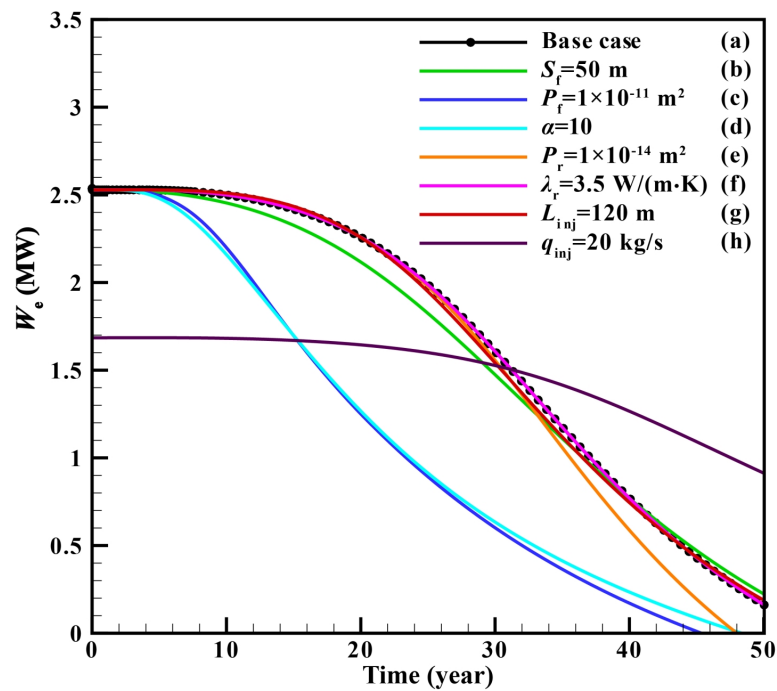
Figure 8. Evolutions of W_e under different parameters over the 50 years.

Over the whole 50 years, λ_r has the least influence on W_e, followed by L_{inj} and S_f. If the lifetime of the EGS project is 30 years, P_r also has little influence on W_e, and the influence of S_f should be considered. It should be noted that the q_{inj} is set to be constant in the numerical simulations of case L_{inj} and case S_f. However, in a practical project, the longer the L_{inj} and the smaller the S_f, the more conducive they are to the increase of q_{inj}.

4.6.4. Bottom-Hole Pressure of Injection Well

Figure 9 shows the evolutions of P_{inj} under different parameters over the 50 years. It illustrates that P_r, S_f, and λ_r have the least influence on P_{inj}. However, α, q_{inj}, and L_{inj} have great influence on P_{inj}. P_f has the greatest effect.
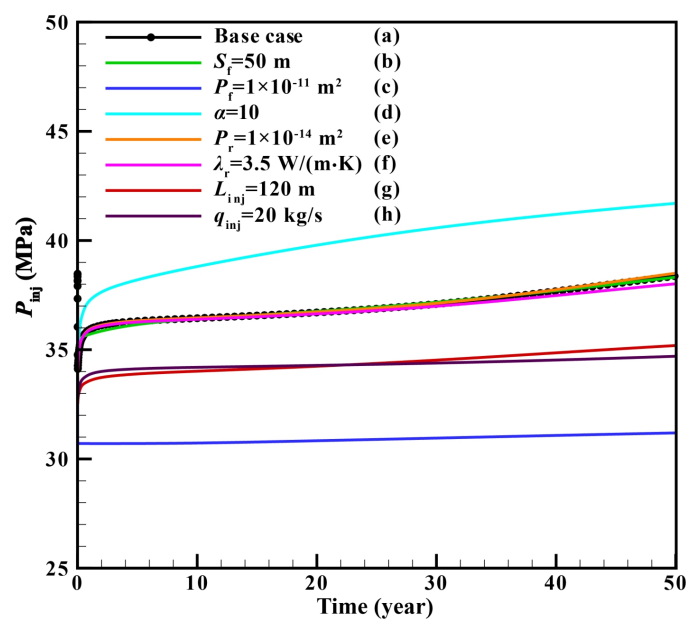

Figure 9. Evolutions of P_{inj} under different parameters over the 50 years.

In the base case, P_{inj} slightly increased from 37.92 MPa up to 38.38 MPa after the 50-year production, increasing by 0.46 MPa (1.2%). When α become 10, the P_{inj} increased from 37.92 MPa to 41.70 MPa over the 50 years, increasing by 3.78 MPa (9.1%). When q_{inj} was 20kg/s, P_{inj} increased from 32.78 MPa to 34.70 MPa, with an increase of 1.92 MPa (5.9%). P_{inj} increased by 0.49 MPa (1.6%), from 30.70 MPa to 31.19MPa, over the 50 years when P_f increased by 100 times. Among all the parameters, P_{inj} increased the most when α become 10 due to a great decrease in vertical permeability compared to the base case. Under the same q_{inj}, the longer the L_{inj}, the lower the P_{inj}. P_{inj} among all the cases met the pressure criterion.

4.6.5. Reservoir Injectivity

The reservoir injectivity, I_{inj}, reflects the stimulation effect of the reservoir permeability. An ideal EGS typically requires an I_{inj} greater than 10 kg/s/MPa. The higher the I_{inj}, the easier it is for water to flow from the injection well to the pumping well at the same pressure difference. It reflects the average flow impedance of the reservoir. I_{inj} is calculated by [1]:

$$I_{inj} = q_{inj}/(P_{inj} - P_{pro}), \tag{12}$$

Figure 10 shows the evolutions of I_{inj} under the different parameters over the 50 years. P_f, L_{inj}, and α are the most important factors. In the base case, I_{inj} ranged from 9.0 to 4.2 kg/s/MPa over the 50 years. In the P_f case, I_{inj} was 1028.2~584.7 kg/s/MPa over the 50 years, which was about 100 times that of the other cases. When the injection length doubled, I_{inj} was 19.7~7.7 kg/s/MPa, which also nearly doubled. In the α case, I_{inj}, 7.6–2.9 kg/s/MPa, was lower than that of the base case.
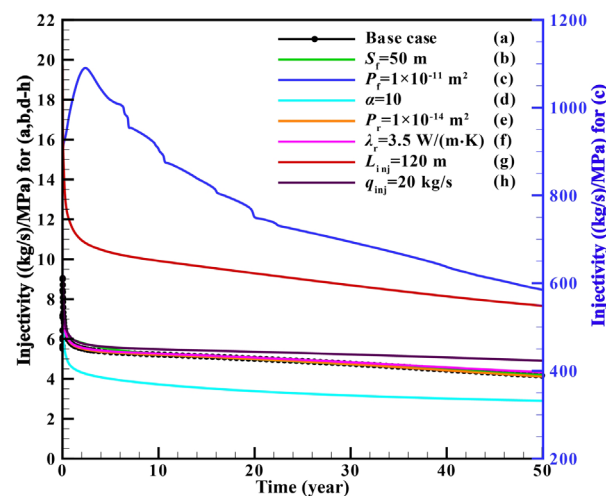
Figure 10. Evolutions of I_{inj} under different parameters over the 50 years.

P_f is directly related to S_f. Assuming that the fracture is flat and smooth, a P_f of 1×10^{-11}m^2 is equivalent to the fracture aperture of 0.05 mm [41]. At present, a fracture aperture of this magnitude mainly depends on the self-supporting of the shear fracture after stimulation. Additionally, in this model, q_{inj} has little influence on I_{inj}. The main reason is that the P_f of 1×10^{-13} m^2 can still smoothly accommodate a 20 kg/s injection flow. If the P_f decreases further, an excess q_{inj} can cause a rapid rise in P_{inj}, resulting in a significant decrease in I_{inj}. Basically, I_{inj} is mainly dependent on the overall permeability of the stimulated reservoir; so, λ_r and P_r have little influence on I_{inj}.

4.6.6. Pump Power

The internal energy consumption, W_p, mainly includes the energy consumption of the injection pump and that of the suction pump [1,8]. W_p mainly refers to the electric

energy consumed to drive water flow through the reservoir. It does not include the energy consumed by injecting water from the surface into the reservoir and pumping water from the reservoir to the surface. If the energy loss due to duct friction and water internal friction is neglected, the pump efficiency η_P is 80%, and the internal energy consumption W_P is Equation (13), based on [8]:

$$W_P = \frac{q(P_{inj} - P_{pro}) - \rho q g(h_1 - h_2)}{\rho \eta_P},$$ (13)

Figure 11 shows the evolutions of W_p under different parameters over the 50 years. P_f is the most important factor, followed by α, q_{inj}, and L_{inj}. Other factors have a slight impact on W_p. Among them, α causes W_p to be higher than that of the base case, while P_f, q_{inj}, and L_{inj} make W_p lower. In the base case, W_p is 0.14~0.30 MW over the 50 years. In the α case, W_p ranges from 0.16 MW to 0.43MW. In the P_f case, W_p is 0.001~0.002 MW. When P_f increases, the reservoir has little resistance to water flow. Water can flow through the reservoir only driven by gravity; so, W_p is extremely low.
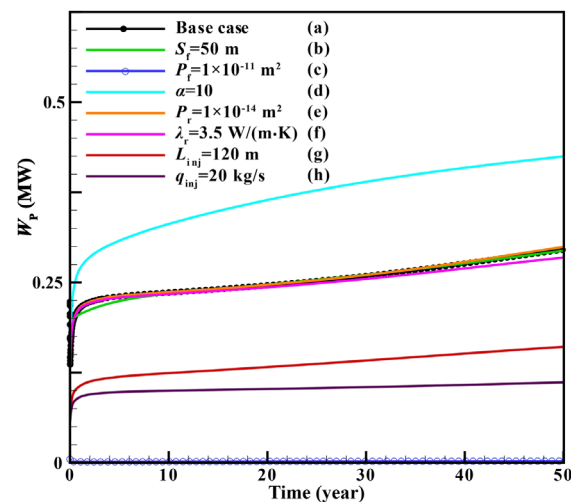

Figure 11. Evolutions of W_p under different parameters over the 50 years.

4.6.7. Coefficient of Performance

The coefficient of performance, η, is defined as the ratio of the total produced power energy to the internal energy consumption [1,33]. It represents the net power generation. Based on Equations (11) and (13), η can be calculated as Equation (14):

$$\eta = W_e/W_p,$$ (14)

Figure 12 shows the evolutions of η under the different parameters over the 50 years. It can be seen that the η of all cases decreased over the entire 50-year operation. P_f is the most important factor affecting η, followed by q_{inj}, L_{inj}, and α. The other factors are less important.

In the base case, η is 18.64~0.64 over the 50 years. In the P_f case, η is 570.19~0, which decreases the fastest mainly because W_e declines too fast. Over the 50 years, the η of the α case was lower than that of the other cases because its W_e declined the most, while W_p increased the most. The decrease of q_{inj} can improve system η, but the curve trend of η is almost unchanged. In the ground source heat pump industry, η is usually expected to be greater than 4. In this simulation, only the case of q_{inj} can meet η larger than 4 during the whole 50 years. The curve patterns of η are in accordance with the previous studies of Refs. [4,8,35].
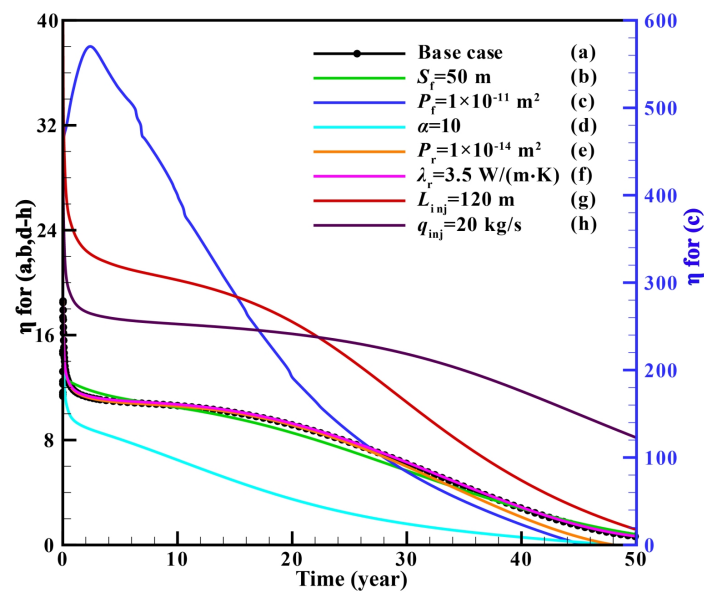
Figure 12. Evolutions of η under different parameters over the 50 years.

4.7. Discussions of Single-Factor Sensitivity Analysis

4.7.1. Effect of Reservoir Factors on Production Performance

The EGS reservoir factors mainly consist of fracture spacing (S_f), fracture permeability (P_f), fracture permeability anisotropy (α), matrix permeability (P_r), and heat conductivity (λ_r).

S_f reflects the development degree of the reservoir fractures. The smaller the S_f, the more developed the fractures. More seepage channels can be selected for water flow. When the q_{inj} is constant and S_f increases from 3 m to 50 m, the flux that each fracture needs to bear increases. Thus, increasing S_f leads to a drop in the produced water temperature and power generation. The larger the S_f is, the more quickly the produced water temperature and power generation decrease, and their stable periods are both shortened. S_f has little effect on the other four indicators. Therefore, the stratum with dense natural fractures should be selected as the target EGS reservoir in practical engineering.

The influence of P_f on each indicator is very large. The greater the P_f, the easier it is for water to pass through the reservoir. According to Darcy's law, when the hydraulic gradient is constant, the water seepage velocity is proportional to the permeability of the reservoir. Thus, when P_f is 100 times greater than that of the base case, the water velocity in the reservoir also increases significantly. The water circulation process would be completed quickly before the cold water absorbed enough heat from the reservoir. The produced water temperature and power generation dropped quickly compared to the base case, and the pump consumption and injectivity increased rapidly. Therefore, it is not advisable to acidify the EGS reservoir too much to widen the apertures of natural fractures. This is likely to lead to a rapid decline in net power generation.

α ($k_x/k_z = 10$) means that the vertical permeability is 10 times lower than that of the base case. When water flows through such fractured reservoirs, it will preferentially reach the production well in the horizontal direction. Thus, the water flow in the vertical direction is greatly restricted. Therefore, the water flow path and the heat exchange area are also smaller than that of the isotropic reservoir. Meanwhile, the water flow through the horizontal direction is greater than that of the base case. In general, the produced water temperature and power generation of an anisotropic reservoir are much lower than that of the base case. In addition, fracture permeability anisotropy increases pump energy consumption greatly.

The greater the P_r, the larger the pores, and therefore the less heat storage per unit volume of rock. When P_r increased by 100 times, the heat storage in the matrix also greatly

decreased. In the dual-porous medium model, the matrix only exchanges heat with the fractures, and there is no heat exchange between the matrixes. In the early stage of the water circulation, the heat in the matrix is continuously transferred to the water flow, and the produced water temperature during this period is almost the same as that of the base case. With the continuous operation of the project, the matrix heat becomes less and less. However, the heat recharge of the wall rock to the reservoir is limited. Therefore, the produced water temperature and power generation both drop faster than that of the base case in the later stage of the project (about 24th year). P_r has little effect on the other four indicators.

The greater the λ_r, the faster the heat conduction from the far field to the reservoir and from the reservoir matrix to the water flow. When λ_r of the rock becomes larger, the stable period of the power generation also becomes longer, indicating that the heat of the reservoir rock is transferred to the fracture water flow more than that of the base case. When entering the descending period, the power generation drops faster than that of the base case due to the excessive extraction of heat from the rock in the early stage. At this time, the temperature difference between the wall rock and the reservoir is not very large; so, the wall rock supplies less heat to the reservoir. As the water continues to circulate, the reservoir with a large λ_r will cool down faster. The heat transfer from the wall rock to the reservoir will increase, and the drop of power generation will begin to slow down. Therefore, the power generation with a large λ_r is slightly higher than that of the base case in the 50th year. Therefore, rock heat conductivity may not be used as an indicator in selecting a target reservoir.

4.7.2. Effect of Operation Factors on Production Performance

The operation factors have a great impact on the EGS production performance. They include injected section length (L_{inj}) and injection rate (q_{inj}).

The lengthening of L_{inj} means the flow rate of a single fracture near the injection well decreases, and the water temperature will become higher. Therefore, the power generation after increasing the length of L_{inj} is a little higher than that of the base case at first. When entering the descending period, because the heat near the injection well is extracted prematurely, the power generation drops faster than that of the base case. It makes the amount of heat supplied to the reservoir by the wall rock higher. The power generation of the extended L_{inj} is a little larger than that of the base case in the 50th year. However, L_{inj} has a great influence on the pump power and the coefficient of performance. The longer the L_{inj}, the lower the pump power and the higher the coefficient of performance. Therefore, in practice, the L_{inj} should be as long as possible.

The lower the q_{inj}, the longer the heat exchange time between the water flow and the reservoir, and therefore the longer the stable period of power generation. The stable periods of power generation under q_{inj} = 20 kg/s and q_{inj} = 30 kg/s are 18 years and 10 years, respectively. Moreover, the smaller the q_{inj}, the slower the drop of power generation during the descending period. q_{inj} has a great influence on the pump power and the coefficient of performance. However, the smaller the q_{inj}, the lower the pump power and the higher the coefficient of performance. Therefore, in practical engineering, the most appropriate q_{inj} should be determined by comprehensive simulations.

4.7.3. Main Factors Affecting Production Performance

According to the above simulation results, it can be seen that the seven parameters selected this time have different effects on the production performance of the EGS. In order to identify their influence degree, a sensitivity analysis was performed based on the above simulation results. The sensitivity, φ, is calculated by:

$$\varphi = \frac{V_{sele} - V_{base}}{V_{base}}, \tag{15}$$

where V_{sele} and V_{base}, respectively, denote the 50-year average of each index under the selected case and the base case. Figure 13 shows the sensitivity analysis results of the different factors on each index.
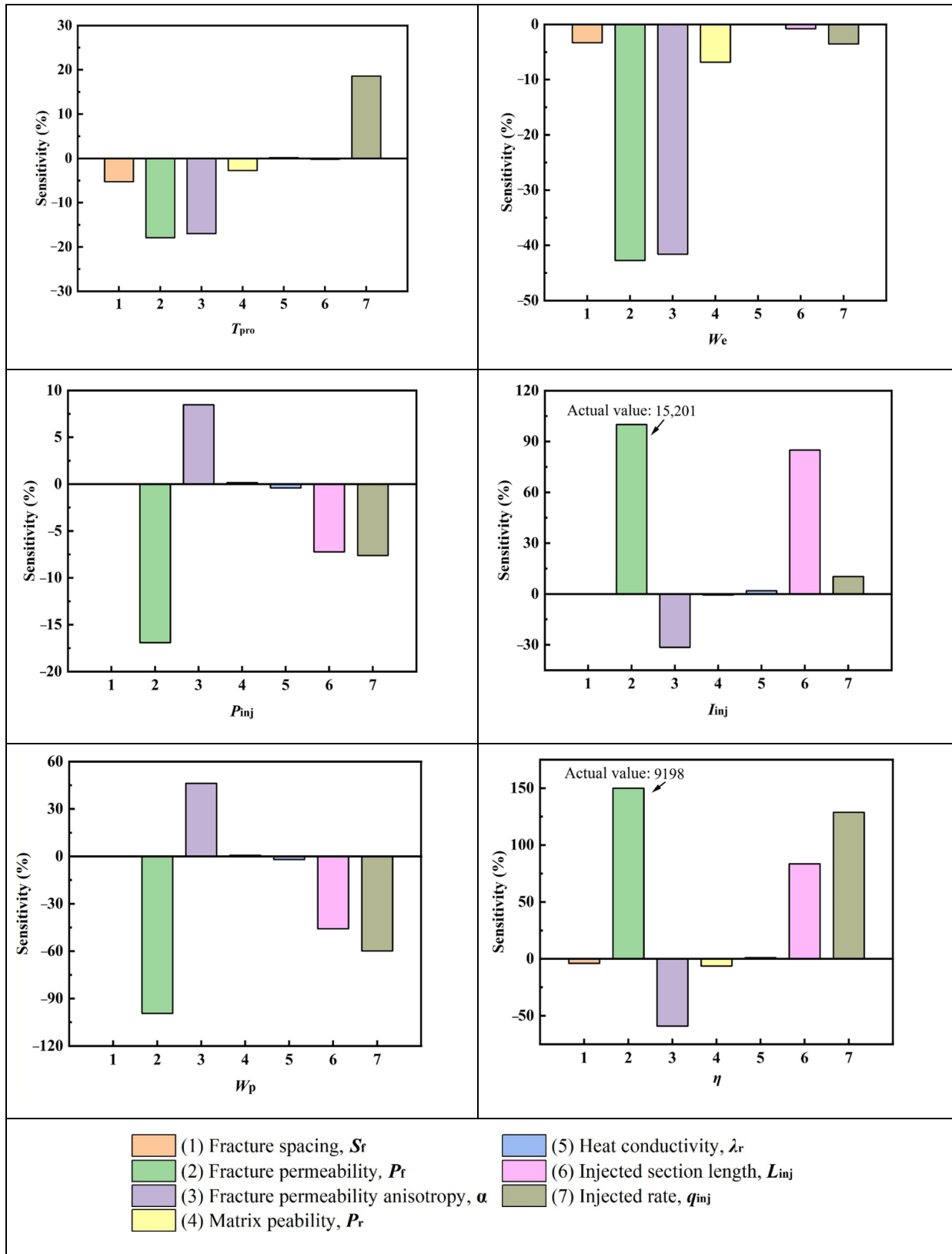

Figure 13. Sensitivity analysis results of different factors on each index.

For T_{pro}, the order of influence degree is as follows: $q_{\text{inj}} > P_{\text{f}} > \alpha > S_{\text{f}} > P_{\text{r}} > L_{\text{inj}} > \lambda_{\text{r}}$. In the long run, the decrease of q_{inj} is beneficial to the increase of T_{pro}. The increase of S_{f}, P_{f}, α, and P_{r} will result in the decrease of T_{pro}. L_{inj} and λ_{r} have little effect on T_{pro}.

For W_{e}, the order of influence degree is as follows: $P_{\text{f}} > \alpha > P_{\text{r}} > q_{\text{inj}} > S_{\text{f}} > L_{\text{inj}} > \lambda_{\text{r}}$. In the long run, the increase of P_{f} and α will obviously reduce W_{e}. Although a higher temperature may be obtained when the injection flow rate decreases, the average annual power generation still decreases.

For P_{inj}, the order of influence degree is as follows: $P_{\text{f}} > \alpha > q_{\text{inj}} > L_{\text{inj}} > \lambda_{\text{r}} > P_{\text{r}} > S_{\text{f}}$. In the long run, the increase of P_{f}, q_{inj}, and L_{inj} will reduce P_{inj}. The increase of α will obviously increase P_{inj}.

For I_{inj}, the order of influence degree is as follows: $P_{\text{f}} > L_{\text{inj}} > \alpha > q_{\text{inj}} > \lambda_{\text{r}} > P_{\text{r}} > S_{\text{f}}$. In the long run, the increase of P_{f} and L_{inj} will significantly increase I_{inj}. The increase of α will decrease I_{inj}.

For W_{p}, the order of influence degree is as follows: $P_{\text{f}} > q_{\text{inj}} > \alpha > L_{\text{inj}} > \lambda_{\text{r}} > P_{\text{r}} > S_{\text{f}}$. In the long run, the increase of P_{f}, q_{inj}, and L_{inj} can significantly reduce W_{p}. The increase of α will increase W_{p}.

For η, the order of influence degree is as follows: $P_{\text{f}} > q_{\text{inj}} > L_{\text{inj}} > \alpha > P_{\text{r}} > S_{\text{f}} > \lambda_{\text{r}}$. In the long run, the increase of P_{f}, q_{inj}, and L_{inj} can significantly increase η. The increase of α will reduce η.

On the whole, the four factors of fracture permeability, fracture permeability anisotropy, injected section length, and injection rate have the greatest influence on the EGS production. W_{e} and η together determine the net generating capacity. It can be seen that only α acts in the same direction on the two indexes, while the other three parameters (P_{f}, q_{inj}, and L_{inj}) act in opposite directions on them. Therefore, multi-factor combination analysis is needed to achieve the optimal combination of W_{e} and η.

5. Multi-Factor Combination Analysis

In practical engineering, the performance index of the EGS is determined by the combination of multi-factors rather than a single factor. Each factor has a certain value range (i.e., multi-level). Therefore, multi-factor and multi-level combination analysis is needed to quantitatively obtain the optimal combination scheme. Generally, the statistical factor analysis (SFA) method needs to match each level of each factor to conduct complete tests, which requires a lot of time. In addition, when the number of the varying parameters in the model becomes large, a large number of numerical samples have to be produced using the SFA, making the optimization study challenging. Compared to the SFA technique, the orthogonal test method can avoid the production of a large number of numerical samples and is more efficient than the SFA technique [21]. The orthogonal test could be used to scientifically arrange and analyze multi-factor and multi-level tests. A standard orthogonal test table is selected based on the number of levels of multi-factors. It can evenly select the representative groups of data in all the test schemes. Through the orthogonal test, the number of experiments greatly is reduced without decreasing the feasibility of the test. Therefore, the orthogonal test is conducted in this part for multi-factor and multi-level combination analysis.

5.1. Orthogonal Test Scheme

As mentioned above, the four factors that had the greatest impact on the EGS productivity were screened out, including fracture permeability, fracture permeability anisotropy, injected section length, and injection rate. For the tests of four factors involving four levels, a complete experiment would test $4 \times 4 \times 4 \times 4 = 256$ trials in total. It is a significant amount of work. In this study, a four-factor and four-level orthogonal test table was adopted. Then, we only need do 16 trials to determine the relative importance of every factor. The distribution of the levels of each factor is shown in Table 6. When P_{f} is 1×10^{-14} m², the bottom-hole pressure increased rapidly from 44.1 MPa to 80.24 MPa in 6 days with the injection rate of 20 kg/s. Thus, the minimum P_{f} was set to 5×10^{-14} m². L_{inj} was set from

30 m to the reservoir height of 300 m. The maximum injection rate was set to 110 kg/s, exceeding the commercial flow rate of 100 kg/s. The maximum level of anisotropy was set as 1000 to consider the influence of a strong anisotropy geology condition. These four levels cover almost all possible scenarios. The orthogonal test scheme is shown in Table 7.

Table 6. Four-factor (A~D) and four-level (1~4).

	Factors			
	A	**B**	**C**	**D**
Level	Fracture Permeability, P_f (m^2)	Fracture Permeability Anisotropy, α	Injected Section Length, L_{inj} (m)	Injection Rate, q_{inj} (kg/s)
1	5×10^{-14}	1	30	20
2	1×10^{-13}	10	120	50
3	1×10^{-12}	100	210	80
4	1×10^{-11}	1000	300	110

Table 7. Orthogonal test scheme.

	Factors			
	A	**B**	**C**	**D**
Test Number	Fracture Permeability, P_f (m^2)	Fracture Permeability Anisotropy, α	Injected Section Length, L_{inj} (m)	Injection Rate, q_{inj} (kg/s)
1	A1 (5×10^{-14})	B1 (1)	C1 (30)	D1 (20)
2	A1 (5×10^{-14})	B2 (10)	C2 (120)	D2 (50)
3	A1 (5×10^{-14})	B3 (100)	C3 (210)	D3 (80)
4	A1 (5×10^{-14})	B4 (1000)	C4 (300)	D4 (110)
5	A2 (1×10^{-13})	B1 (1)	C2 (120)	D3 (80)
6	A2 (1×10^{-13})	B2 (10)	C1 (30)	D4 (110)
7	A2 (1×10^{-13})	B3 (100)	C4 (300)	D1 (20)
8	A2 (1×10^{-13})	B4 (1000)	C3 (210)	D2 (50)
9	A3 (1×10^{-12})	B1 (1)	C3 (210)	D4 (110)
10	A3 (1×10^{-12})	B2 (10)	C4 (300)	D3 (80)
11	A3 (1×10^{-12})	B3 (100)	C1 (30)	D2 (50)
12	A3 (1×10^{-12})	B4 (1000)	C2 (120)	D1 (20)
13	A4 (1×10^{-11})	B1 (1)	C4 (300)	D2 (50)
14	A4 (1×10^{-11})	B2 (10)	C3 (210)	D1 (20)
15	A4 (1×10^{-11})	B3 (100)	C2 (120)	D4 (110)
16	A4 (1×10^{-11})	B4 (1000)	C1 (30)	D3 (80)

5.2. Orthogonal Test Results

Table 8 lists the simulation results of the orthogonal test according to Table 7. According to the single-factor simulation curve in Section 4, it can be seen that the variation path of W_e may be different in different situations. Even if both scenarios produce the same amount of electricity in the 50th year, they may produce very different amounts over the entire 50 years. So, the 50-year average of each index is needed. In addition, the initial values of some indexes, such as η and I_{inj}, may differ greatly from the final values in the 50th year. The project may be no longer operational before 50 years. Only using the 50-year average cannot accurately represent the influence of the test. Therefore, the average annual value is mainly used for comparison, and the value at the end of the simulation is used for auxiliary judgment.

Table 8. Orthogonal test results. V_{End} and $V_{Ave.}$ denote the value at the end of simulation and the average annual value of each index, respectively.

| Test Number		Index					
		Power Generation, W_e	Coefficient of Performance, η	Production Temperature, T_{pro}	Injectivity, I_{inj}	Bottom-Hole Pressure, P_{inj}	Pump Power, W_P
1	V_{End}	1.00	2.38	176.46	1.13	30.69	0.42
	$V_{Ave.}$	1.45	3.63	208.11	1.17	30.61	0.40
2	V_{End}	−1.60	−0.88	52.87	1.79	60.27	1.81
	$V_{Ave.}$	0.33	0.21	110.62	2.12	55.82	1.54
3	V_{End}	−1.24	−0.28	77.53	1.96	74.69	4.38
	$V_{Ave.}$	0.49	0.20	110.07	2.32	68.63	3.77
4	V_{End}	−3.35	−1.01	54.78	5.01	55.83	3.30
	$V_{Ave.}$	−1.44	−0.37	81.09	5.62	53.46	2.99
5	V_{End}	−2.62	−1.55	51.67	4.68	49.62	1.69
	$V_{Ave.}$	−0.36	0.13	93.97	5.42	46.90	1.48
6	V_{End}	-	-	-	-	-	-
	$V_{Ave.}$						
7	V_{End}	1.11	35.26	183.40	17.43	33.65	0.03
	$V_{Ave.}$	1.46	51.99	208.79	19.28	33.44	0.03
8	V_{End}	−0.86	−0.31	222.41	1.22	74.70	−0.86
	$V_{Ave.}$	0.67	0.57	223.83	1.69	64.89	0.67
9	V_{End}	−4.96	−20.56	32.41	45.66	36.71	0.24
	$V_{Ave.}$	−3.74	−16.04	49.37	48.45	36.00	0.22
10	V_{End}	−2.29	−24.98	57.69	95.71	34.60	0.09
	$V_{Ave.}$	-0.88	−7.97	84.32	110.12	34.12	0.08
11	V_{End}	−1.27	−2.08	62.2	4.39	45.92	0.61
	$V_{Ave.}$	0.88	2.80	126.6	5.15	42.59	0.50
12	V_{End}	0.43	5.55	132.38	2.65	38.82	0.16
	$V_{Ave.}$	1.14	12.41	185.98	3.63	36.93	0.11
13	V_{End}	−1.68	−377.26	50.34	897.44	33.10	0.0038
	$V_{Ave.}$	−0.91	−439.38	73.60	892.88	32.92	0.0038
14	V_{End}	0.05	18.77	104.76	22.34	32.68	0.0024
	$V_{Ave.}$	0.52	420.36	140.23	22.90	32.58	0.0019
15	V_{End}	−4.28	−25.12	41.83	40.07	36.94	0.17
	$V_{Ave.}$	−1.71	−6.44	77.13	41.85	35.94	0.15
16	V_{End}	−3.17	−2.67	39.48	6.04	53.71	1.19
	$V_{Ave.}$	−0.88	0.05	83.07	7.23	48.87	0.99

From Table 8, based on the average annual value of the 16 tests, W_e ranges from −3.47 MW to 1.46 MW; η ranges from −439.38 to 420.36; T_{pro} ranges from 49.37 °C to 223.83 °C; I_{inj} ranges from 1.17 to 892.88; P_{inj} ranges from 30.61 to 68.63; and W_P ranges from 0.0019 MW to 3.77 MW. It can be seen that the different combinations have great influence on the heat transfer performance, and it is difficult to meet all six indexes at the same time. For example, although the W_e of test 1 is good, its η and I_{inj} are low. For W_e, the better combinations include test 7, test 1, and test 12. For η, the better combinations include test 7 and test 14. Their common characteristic is an injection rate of 20 kg/s. All six indexes of test 7 are good, indicating that the level of all the factors in scheme 7 is better combined at this time. The negative value of W_e in Table 8 is because the selected organic working medium isobutene cannot generate power when its temperature is lower than 105.36 °C, as mentioned in Section 4.6.1. In the practical engineering, W_e and η cannot be

negative. However, in order to directly reflect the influence of each factor, their theoretical negative values are adopted this time. In addition, for test 6, the injection rate of 110 kg/s was too high for the fracture permeability of 1×10^{-13} m^2, resulting in a rapid increase of P_{inj}; so, test 6 has no data. Similarly, test 3 and test 8 only run to 15.8 years and 25.2 years, respectively, due to the excessive pressure growth.

5.3. Discussions of Multi-Factor Combination Analysis

5.3.1. Effect of Main Factors on Production Performance

The ultimate purpose of heat extraction is to generate electricity; so, net power generation is the first benefit indicator to be concerned with and is determined by power generation (W_e), pump power (W_p), and the coefficient of performance (η). Injection pressure is allowed to grow as long as it is not so high as to exceed the strength capacity of the pump and pipeline. In order to further explore which factor plays a dominant role in the multi-parameter combination, we sorted out the results in Table 8 according to W_e, W_p, and η (Figure 14).
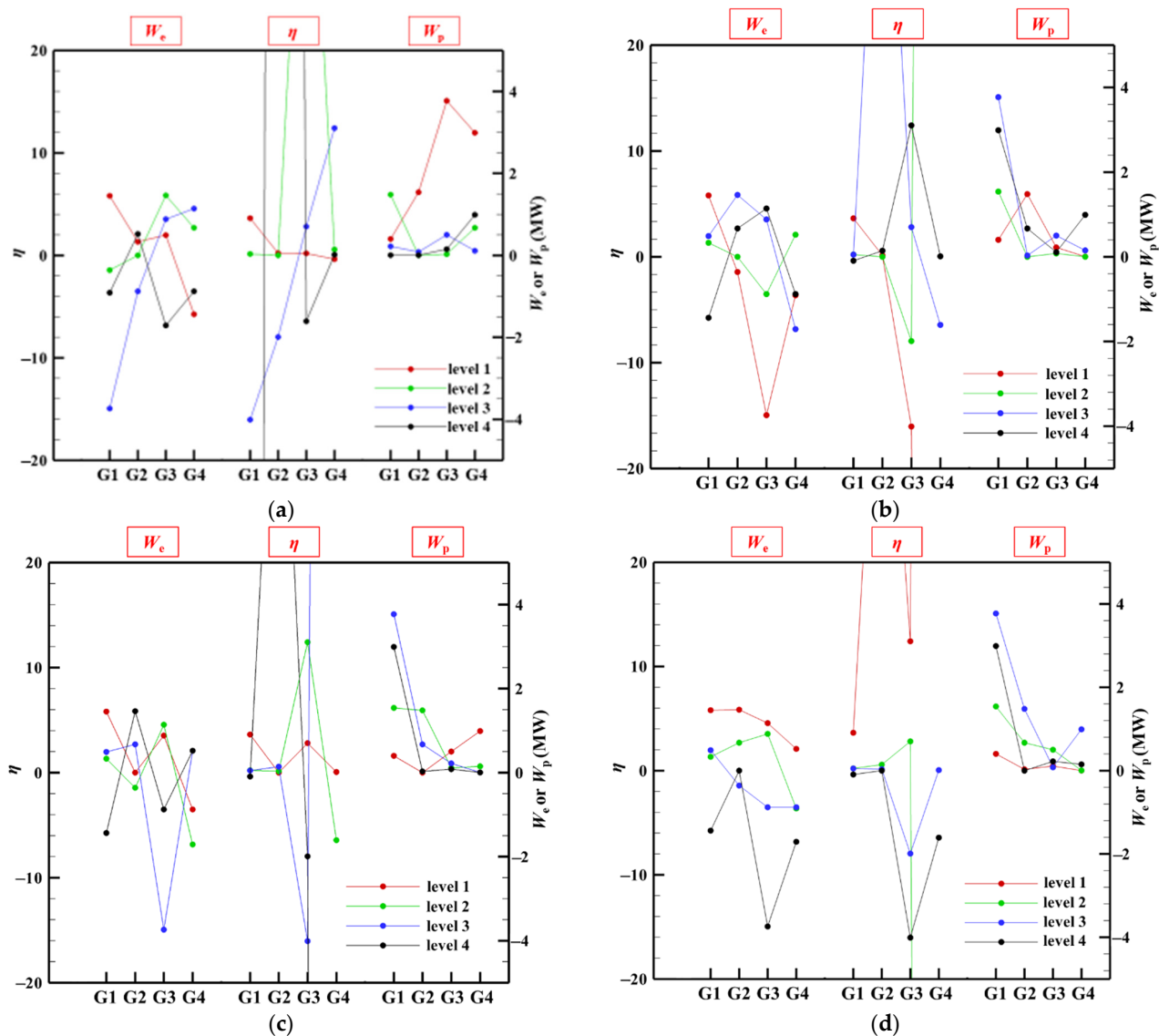
Figure 14. Variations of W_e, W_p, and η at four levels of different factors based on the results in Table 8. G1–G4 represent the results of the four tests at each level: (**a**) fracture permeability; (**b**) fracture permeability anisotropy; (**c**) injected section length; and (**d**) injection rate.

For the fracture permeability (Figure 14a), it can be seen that W_e varies greatly even though it is for the same level. This means that even when the fracture permeability is selected to the optimal value, the resulting W_e may be very low if the other parameters do not match the fracture permeability. The variation range of η at the same level may be very different, indicating that a different fracture permeability may have a great impact on η. The W_p of the other three levels, except that of level 1, does not change much. Considering the three indicators, the best cases at levels 1~4 are G1, G3, G4, and G2, respectively. From level 1 to level 4, W_e, η, and W_p do not increase or decrease as the fracture permeability increases, indicating that it is not necessary to increase fracture permeability too much in the actual reservoir stimulation. Depending on other parameters, even small fracture permeability can generate significant W_e (i.e., G1 at level 1 and G3 at level 2). However, when the fracture permeability is low (level 1), W_p is higher in most cases than that at the other levels, and overall η is higher than that at the other levels. When fracture permeability is large (level 4), W_e is also small. Therefore, the overall fracture permeability should not be too low or too high.

For the fracture permeability anisotropy (Figure 14b), it can be seen that W_e varies greatly even though it is for the same level, indicating that fracture permeability anisotropy does not dominate. If the values of the other factors do not match, productivity will also be affected. With the increase in fracture permeability anisotropy (from level 1 to level 4), there is no obvious increase or decrease of each indicator. Even if the anisotropy is very large, it is possible to obtain larger W_e as long as the other parameters are well matched. Considering the three indicators, the best cases at level 1~4 are G1, G4, G2, and G3, respectively. It also shows that even though the actual fracture permeability anisotropy varies greatly, we only need to find other parameters matching it. It is not necessary to stimulate the reservoir permeability to be isotropic.

For the injected section length (Figure 14c), it can be seen that W_e varies greatly even though it is for the same level. The injected section length does not dominate. The fluctuation of the three indicators of level 1 is relatively small. This means that when the injected section length is small, the other parameters have difficulty playing a large role. At this time, if the injected section length is not increased, the EGS production performance cannot be improved. The three indicators at level 3 and level 4 fluctuate greatly, indicating more possibility of combination with the other factors. Therefore, in practical engineering, the injected section length should be larger. Ref. [42] shows that a larger L_{inj} enhances heat extraction when L_{inj} is less than the reservoir height. The regularity of our results is consistent with Ref. [42].

For the injection rate (Figure 14d), W_e and η obviously decrease as injection rate increases (from level 1 to level 4), regardless of whether the other factors are matched. The lower the injection rate, the lower the W_p. Moreover, as the injection rate increases, W_e and η drop rapidly to negative values. It indicates that the produced water temperature drops too fast with the increase in the injection rate. All three indicators of level 1 are the best of the four levels. Thus, the injection rate determines in all factors, and the smaller the better. Therefore, in practical engineering, special attention should be paid to the value of the injection rate, which should not be too large.

5.3.2. Order of Main Factors and Optimal Combination

In order to quantitatively determine the order of influence degree of each factor, a range analysis was carried out based on the orthogonal test results. Table 9 lists the range analysis results. The greater the range, the more important the influence of the factors on the production evaluation index [22,27].

Table 9. Range analysis results of the orthogonal test. For simplicity, only all k_i values of W_e and η are listed in the table. The other indexes only give R and rank results.

Index	Value	Factors			
		A	**B**	**C**	**D**
W_e	k_1	0.21	−0.89	0.48	1.26
	k_2	0.59	−0.01	−0.03	0.24
	k_3	−0.53	0.28	−0.52	−0.41
	k_4	−0.75	−0.01	−0.44	−2.30
	R	1.34	1.17	0.10	3.56
	Rank	2	3	4	1
	Better level		$A_2B_3C_1D_1$		
η	k_1	−112.92	0.92	2.16	124.52
	k_2	137.53	17.56	4.00	−108.95
	k_3	12.14	0.22	101.27	−1.8975
	k_4	5.59	−6.35	−98.93	−7.62
	R	250.45	23.92	200.21	233.47
	Rank	1	4	3	2
	Better level		$A_2B_2C_3D_1$		
T_{pro}	R	82.02	45.69	27.31	125.04
	Rank	2	3	4	1
I_{inj}	R	238.41	232.21	252.46	213.49
	Rank	2	3	1	4
P_{inj}	R	15.30	13.85	12.04	16.82
	Rank	2	3	4	1
W_p	R	1.96	0.66	0.54	1.45
	Rank	1	3	4	2

For T_{pro}, the order of influence degree is as follows: $q_{inj} > P_f > \alpha > L_{inj}$. This result is consistent with that of the single-factor sensitivity analysis.

For W_e, the order of influence degree is as follows: $q_{inj} > P_f > \alpha > L_{inj}$. In comparison with the result of the single-factor sensitivity analysis, only the order of q_{inj} and P_f has changed.

For P_{inj}, the order of influence degree is as follows: $q_{inj} > P_f > \alpha > L_{inj}$. In comparison with the result of the single-factor sensitivity analysis, only the order of q_{inj} and P_f has changed.

For I_{inj}, the order of influence degree is as follows: $L_{inj} > P_f > \alpha > q_{inj}$. In comparison with the result of the single-factor sensitivity analysis, only the order of L_{inj} and P_f has changed.

For W_p, the order of influence degree is as follows: $P_f > q_{inj} > \alpha > L_{inj}$. This result is consistent with that of the single-factor sensitivity analysis.

For η, the order of influence degree is as follows: $P_f > q_{inj} > L_{inj} > \alpha$. This result is consistent with that of the single-factor sensitivity analysis.

On the whole, the rank results of the orthogonal test are almost the same as those of single-factor sensitivity. It proves the accuracy of the simulation results. In the actual EGS project, the two most concerned indicators are W_e and η. According to Table 9, the better level combination of these two indicators is $A_2B_3C_1D_1$ and $A_2B_2C_3D_1$, respectively. From the orthogonal results listed in Table 8, the optimal combination is test 7 ($A_2B_3C_4D_1$). The comparison of these three combinations and the results are shown in Figure 15. The W_e of $A_2B_3C_1D_1$, $A_2B_2C_3D_1$, and $A_2B_3C_4D_1$ over the 50 years are 1.69 MW~1.04 MW, 1.69 MW~0.68 MW, and 1.69 MW~1.11 MW. Between 0 and 42.3 years, the W_e of $A_2B_3C_1D_1$ was consistently higher than that of $A_2B_3C_4D_1$. The η of $A_2B_3C_1D_1$, $A_2B_2C_3D_1$, and $A_2B_3C_4D_1$ over the 50 years are 12.53~1.70, 14.59~12.70, and 120.26~35.26. Although the W_e of $A_2B_3C_1D_1$ is overall higher than that of $A_2B_3C_4D_1$, the η of $A_2B_3C_1D_1$ is much lower than that of $A_2B_3C_4D_1$. Thus, considering W_e and η comprehensively, the optimal scheme is

$A_2B_3C_4D_1$. Based on the above results, this indicates that the optimal EGS reservoir should have moderate fracture permeability and moderate fracture permeability anisotropy; the injected section length should be large; and the injection rate should be moderate.
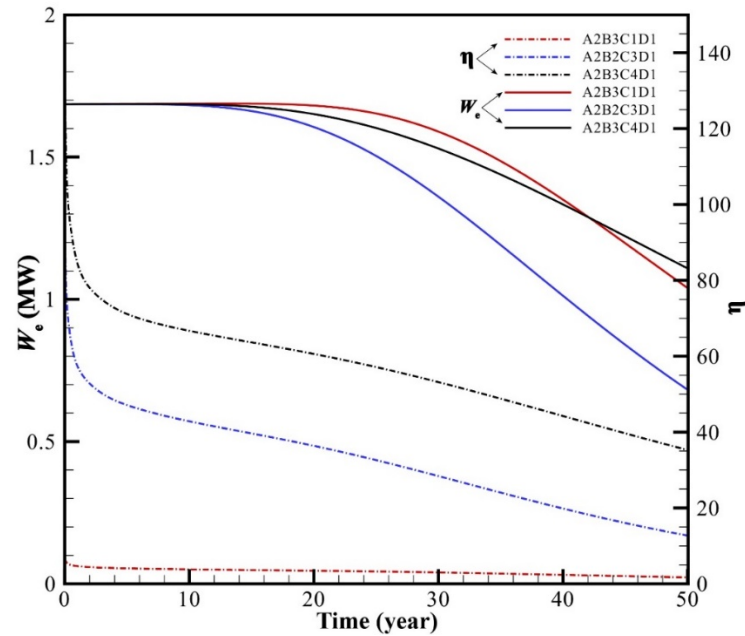

Figure 15. Simulation results of three combinations of $A_2B_3C_1D_1$, $A_2B_2C_3D_1$, and $A_2B_3C_4D_1$.

### 5.3.3. Optimal Scheme Considering Fracture Permeability Anisotropy

In practice, it is difficult to control and determine fracture permeability anisotropy (α) because it is greatly affected by in situ stress and natural fracture distribution. To study the effect of fracture permeability anisotropy on the production performance, a single-factor three-level test was specially arranged. The results are listed in Table 10. With the increase of α, W_e and T_{pro} increase first and then decrease, while P_{inj} and W_p keep growing. So, η decreases downwards. All the cases in Table 10 comply with the temperature and pressure criteria. If permeability anisotropy can be controlled during reservoir stimulation, the optimal strategy is still test $A_2B_3C_4D_1$ ($\alpha = 100$). If permeability anisotropy is not controlled, the 50-year average W_e, η, and I_{inj} with $A_2C_4D_1$ are likely to be 1.23 MW~1.46 MW, 11.42~67.50, and 14.28~20.92, respectively. In addition, it can be seen that the 6 indicators of these 4 tests in Table 10 are all good and are all better than that of the 15 tests, except test 7 in Table 8. Therefore, this proves that the optimization combinatorial scheme of EGS can be achieved through the orthogonal test and range analysis.

Table 10. Results of single-factor (α) three-level test based on test $A_2B_3C_4D_1$.

Test		W_e	η	T_{pro}	I_{inj}	P_{inj}	W_p
$A_2B_1C_4D_1$ ($\alpha = 1$)	V_{End}	0.97	69.29	173.07	19.63	33.03	0.014
	$V_{Ave.}$	1.23	64.74	192.28	20.92	33.03	0.019
$A_2B_2C_4D_1$ ($\alpha = 10$)	V_{End}	1.02	63.75	177.18	19.29	33.1	0.016
	$V_{Ave.}$	1.35	67.50	201.02	20.69	33.07	0.02
$A_2B_3C_4D_1$ ($\alpha = 100$)	V_{End}	1.11	35.26	183.4	17.43	33.65	0.03
	$V_{Ave.}$	1.46	51.99	208.79	19.28	33.44	0.03
$A_2B_4C_4D_1$ ($\alpha = 1000$)	V_{End}	1.01	6.20	174.88	12.35	38.83	0.163
	$V_{Ave.}$	1.37	11.42	202.77	14.28	37.06	0.12

5.3.4. Optimal Scheme Considering Injection Rate

As mentioned above, the injection rate is decisive even in a multi-factor combination. Meanwhile, the lower the injection rate, the greater the average power generation over 50 years. In order to explore the lower limit of the optimal injection rate, we conducted simulations of net power generation ($W_e - W_p$) under different injection rates based on test $A_2B_3C_4D_1$, as shown in Figure 16. The results show that with the decrease in the injection rate, the stable period of net power generation gradually lengthens. The decreasing rate of the net power generation during the descending period also slows down. However, in the initial period, the net power generation is still higher when the injection rate is higher. Thus, the net power generation at 30 kg/s is greater than that at 20 kg/s up to 34.2 years. The net power generation at 20 kg/s was consistently greater than that at 15 kg/s for the entire 50 years. The intersection of the two curves occurred 50 years later. The net power generation at 10 kg/s is almost constant over a 50-year period. Therefore, the choice of optimal injection rate also depends on the life of the project. The injection rate should not be excessive if the EGS project life is required to be longer.
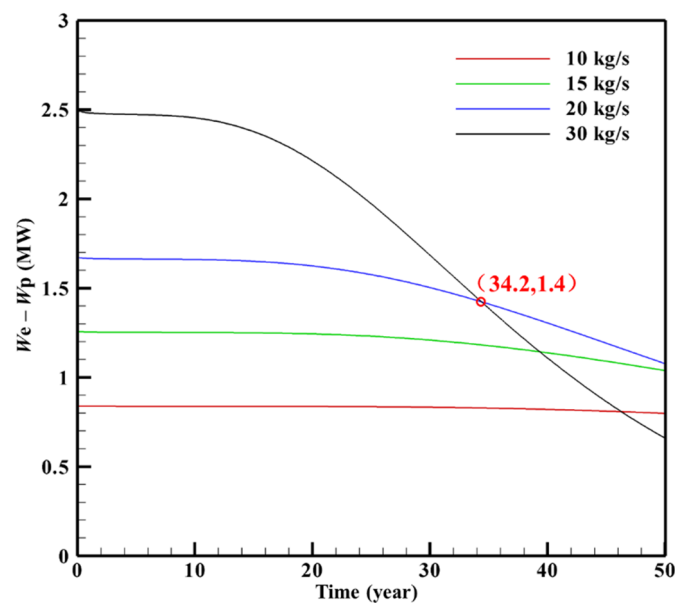
Figure 16. Comparison of net power generation ($W_e - W_p$) under different of injection rates based on test $A_2B_3C_4D_1$.

The commercial injection rate of the EGS is expected more than 100 kg/s. According to the above simulation results, when the injection rate reaches 100 kg/s, the produced water temperature and the power generation both decline quickly. Meanwhile, the injection pressure will also rise rapidly, which can easily cause high pump pressure, causing great difficulties to the operation. If a commercial rate (100 kg/s) is to be obtained, the permeability of the reservoir fracture network needs to be stimulated to be higher. Meanwhile, in order to ensure that the production temperature is both high and stable, it is necessary to further increase the volume of the EGS reservoir.

5.3.5. Well Layout Mode

The EGS reservoir volume in this paper is 0.54×10^8 m^3. Sanyal and Butler [43] proposed that the stimulated volume should exceed 1×10^8 m^3 for the EGS. The EGS reservoir volume needs to be increased further. If the created EGS reservoir is too long, a large flow resistance needs to be overcome in order to drive water through the reservoir. Considering the symmetry of hydraulic fracturing, the triplet-well straight-line mode with one injector and two producers is recommended according to case $A_2B_3C_4D_1$ (Figure 17). Well spacing is 600 m, and the total EGS reservoir volume reaches 1.08×10^8 m^3. During reservoir

stimulation, fractures mostly extend parallel to the direction of maximum principal stress. Thus, the direction of the well connection line is set in the same direction as the maximum principal stress in the study area (N51°). The injection rate is 40 kg/s and the flow rate from each production well is 20 kg/s. In actual engineering, more fluid may need to be injected to compensate for the fluid loss. The 50-year average of W_e, η, and I_{inj} with this triplet-well mode can reach 2.46 MW~2.92 MW, 11.42~67.50, and 14.28~20.92, respectively.
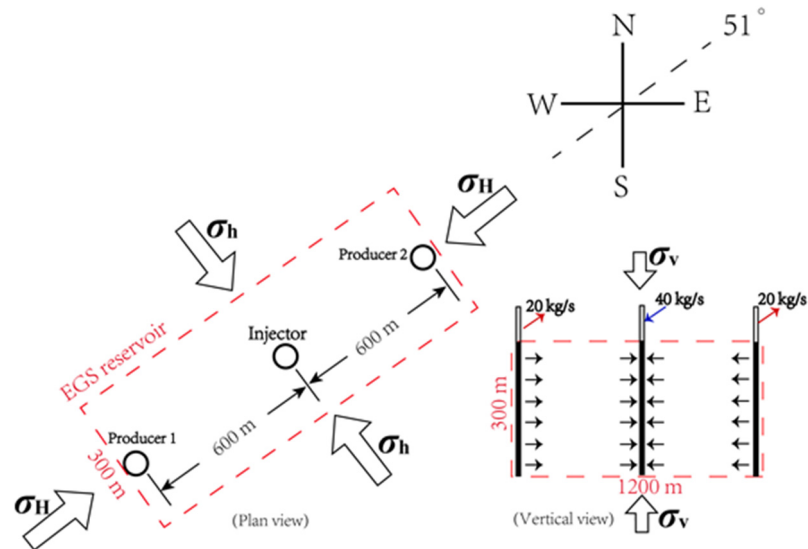

Figure 17. Schematic diagram of optimal well layout designed according to case $A_2B_3C_4D_1$.

5.3.6. Optimal Scheme Considering Injection Water Temperature

In this study, groundwater is assumed to be used as the injection water, with an injection temperature of 10 °C. In practical projects, the reinjection water may have different temperatures after surface power generation and stepped heat exchange. To further optimize the scheme, the effect of different injection water temperatures on productivity was studied. Figure 18 shows the comparison of the production index under different values of injection temperature in the 50th year, based on test $A_2B_3C_4D_1$.
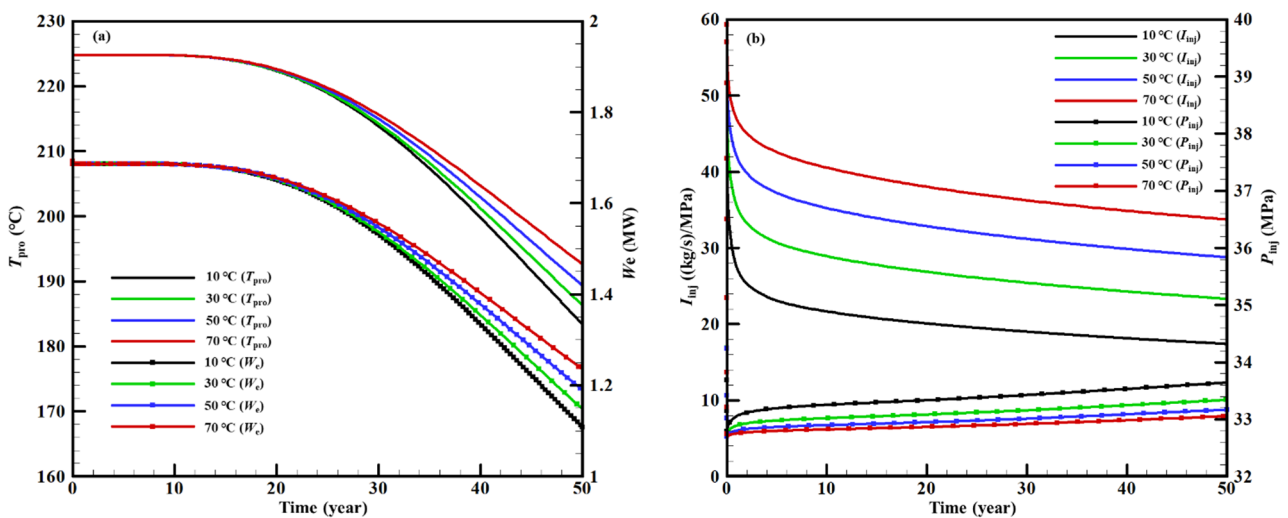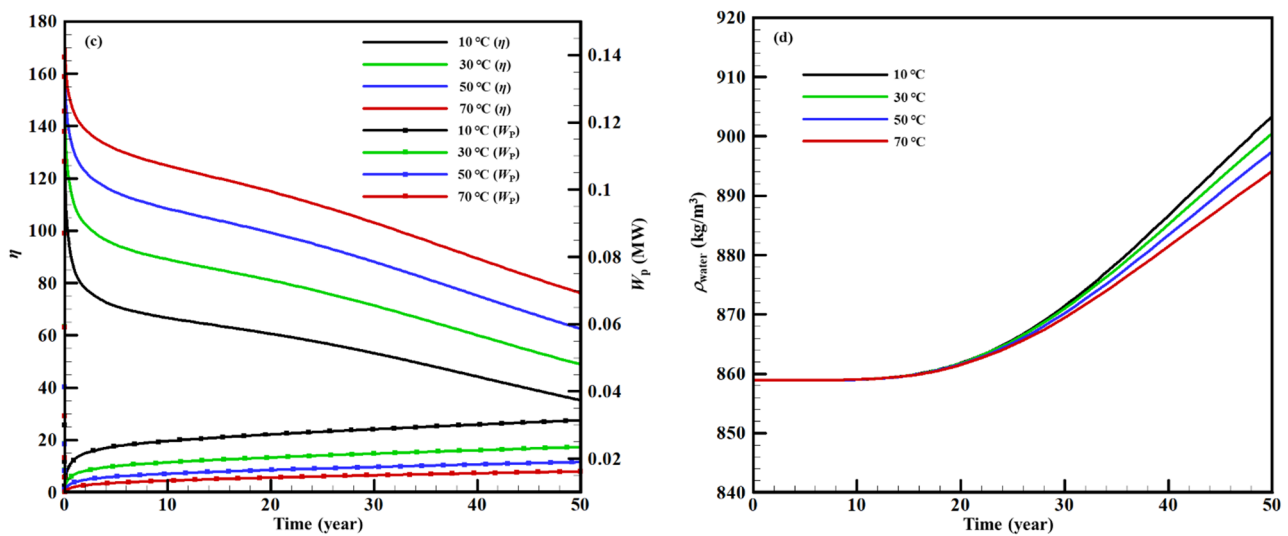

Figure 18. *Cont.*

Figure 18. Comparison of production index under different injection temperature in the 50th year based on test $A_2B_3C_4D_1$. The production index include T_{pro} and W_e (**a**), I_{inj} and P_{inj} (**b**), η and W_p (**c**), and production water density, ρ_{water} (**d**).

The temperature difference between the reservoir and the injected water of the four cases is higher than 100 °C. It results in a small difference in their stable periods of T_{pro} and W_e (Figure 18a). During the decline stage, a high injection temperature causes a slow drop of T_{pro} and W_e. Increasing the injection temperature will definitely increase T_{pro} and W_e; however, the increase in the injection temperature also requires extra energy. The appropriate injection temperature should be determined in accordance with the water source condition and the engineering requirement.

With the increase in the injection temperature, P_{inj} and W_p both decrease. P_{inj} is the function of (μ/ρ), which is also the function of temperature. As heat production continues, the reservoir temperature continually declines; (μ/ρ) significantly increases when the temperature declines (Figure 18d). The higher injection temperature causes the production temperature to drop more slowly. Thus, P_{inj} and W_p both increase slowly when the injection temperature is higher (Figure 18b,c). Finally, I_{inj} and η are both improved according to Equations (12) and (14).

5.3.7. Space Variation of Reservoir Temperature Field

Figure 19 shows the profiles of the space variations of the reservoir temperature fields over the 50 years ($y = 350$m) ($a\sim e$) and the temperature plan in the 50th year ($z = 350$m) (f). The results are based on test $A_2B_3C_4D_1$ with an injection temperature of 70 °C. As can be seen from the profile, with the cold water gradually injected into the reservoir, the cold front continues to move towards the pumping well. Generally, the density of the injected cold water is large; so, its downward speed is high under the gravity drive. Because the water injection section and pumping section are located at the same depth in this study, the vertical diffusion velocity of the cold halo is nearly the same as the horizontal diffusion velocity (Figure 19a–e). Thus, the cold front almost uniformly moves horizontally from the injection well to the pumping well, and the heat extracted from the whole reservoir is sufficient. It can be seen from Figure 19f that after 50 years of operation, the lateral influence range of thermal extraction on wall rock is about 99 m on each side and that of the injection well and pumping well sides is 148 m and 24 m, respectively. Cooling does not affect the boundary of the model in this simulation, indicating that the size and boundary conditions of this model are reasonable.
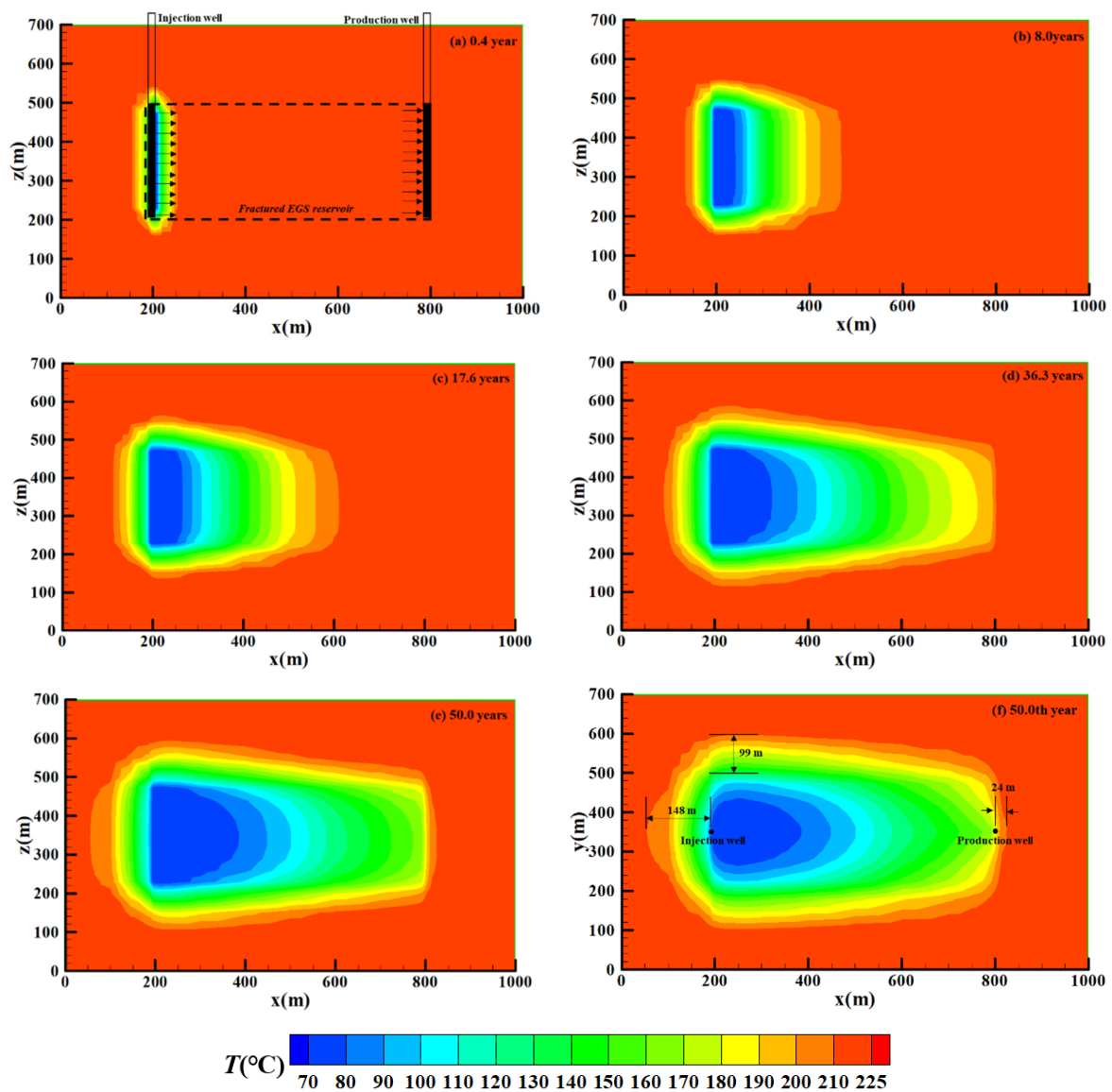
Figure 19. Profiles of space variations of reservoir temperature fields over 50 years (y = 350 m) (**a–e**) and the temperature plan in the 50th year (z = 350 m) (**f**). The results are based on test $A_2B_3C_4D_1$ with injection temperature of 70 °C.

6. Conclusions

Based on the geothermal geological characteristics of the Qiabuqia area, Gonghe Basin, a hydraulic-thermal coupled numerical model was established by using the MINC method. In order to explore the optimal mining strategy of the fractured EGS reservoir, we numerically investigated the influence of seven single factors on heat production and conducted an optimization of multi-factor combinations by an orthogonal test. The following conclusions were drawn:

(1) The Gonghe Basin possess a good geothermal structure. The molten layer in the depth interval of 15~35 km may be the heat source. The widely distributed huge-thick high-temperature granite formation is an ideal target reservoir for HDR. The cap rocks are mainly mudstone and sandstone, which have the characteristics of low heat conductivity. The complex geological structure has produced many deep large faults, which can serve as heat conduction channels. Therefore, there has formed a relatively shallow high-temperature HDR reservoir in the Gonghe Basin.

(2) For single-factor sensitivity analysis, when q_{inj} was constant, the increase of S_f had a slight influence on T_{pro} and W_e. P_f had the greatest influence on the production performance among all the factors. For the condition with $\alpha = 10$, W_e declined the fastest, while W_p rose the fastest, resulting in the lowest η. The increase of P_r had a slight influence on T_{pro} and W_e in the later stage of the project. λ_r was the least influential of all the parameters. Increasing L_{inj} had little influence on T_{pro} and W_e but had great influence on P_{inj} and W_p. When q_{inj} decreased, the early W_e decreased due to the flow rate limitation although T_{pro} declined much more slowly. Meanwhile, W_p decreased and η increased significantly. Therefore, the biggest influence factor on the W_e value was the overall permeability of the fractured reservoir. For η, P_f was the most important factor, followed by q_{inj}, L_{inj}, and α.

(3) The four factors of fracture permeability, fracture permeability anisotropy, injected section length, and injection rate had the greatest influence on the EGS production. For the multi-factor sensitivity analysis, the order of influence degree on W_e was $q_{inj} > P_f > \alpha > L_{inj}$. The order of influence degree on η was $P_f > q_{inj} > L_{inj} > \alpha$. On the whole, the rank results of the orthogonal test are almost the same as those of single-factor sensitivity.

(4) Different factor combinations have great influence on the heat transfer performance. The multi-factor and multi-level combination optimization is needed and the optimization scheme of the EGS can be achieved through the orthogonal test and range analysis.

(5) For reservoir stimulation, the stratum with dense natural fractures should be selected as the target EGS reservoir. It is not advisable to acidify the EGS reservoir too much to widen the apertures of natural fractures. This is likely to lead to a rapid decline in net power generation. Fracture permeability anisotropy will increase pump energy consumption, but this adverse effect can be greatly reduced if the other parameters are well matched. Matrix permeability and heat conductivity may not be used as an indicator in selecting a target reservoir.

(6) For project operation, the injected section length should be as long as possible. The injection rate plays a major role in all factors. Special attention should be paid to the value of the injection rate, which should not be too large. The appropriate injection temperature should be determined in accordance with the water source condition and the engineering requirement. If a commercial rate (100 kg/s) is to be obtained, the permeability of the reservoir fracture network needs to be stimulated to be higher. Meanwhile, in order to ensure that the production temperature is both high and stable, it is necessary to further increase the volume of the EGS reservoir.

In practical EGS projects, we suggest that one should be very careful when choosing which formation to use as the EGS target reservoir. Firstly, the high-temperature reservoir should be selected, as far as possible, and the reservoir size should be created as large as possible. This can ensure the lower limit of the EGS reservoir productivity. As for optimization, the best way is to obtain as much reservoir information as possible and conduct sufficient numerical simulations. In this study, considering the complexity of the actual project, we simplified the numerical model. Only the coupling of the hydraulic-thermal effect was considered and water losses in the reservoir were neglected. However, the rock mechanical deformation and the water–rock chemical reaction must be considered during the long-term operation of the EGS. Additionally, the logging data of the distribution characteristics of the facture spacing, aperture, and orientation should be collected to establish a more realistic hydraulic–thermal–mechanical–chemical model in the future.

Author Contributions: Conceptualization, Y.Z. and L.G.; methodology, L.G.; software, J.Z.; validation, L.S.; writing—original draft preparation, S.C.; writing—review and editing, Y.Z.; supervision, J.Z. All authors have read and agreed to the published version of the manuscript.

Institutional Review Board Statement: Not applicable. The study did not involve humans or animals.

Informed Consent Statement: Not applicable. The study did not involve humans.

Data Availability Statement: Some or all of the data and the models generated or used during the study are available from the corresponding author by request.

Conflicts of Interest: The authors declare no conflict of interest.

Nomenclature

C_R	Rock specific heat, J/(kg·K)	h_β	Specific enthalpy in phase β, J/kg
F	Mass or heat flux, kg/m^2 or W/m^2	t	Time, s
I_{inj}	Injectivity, kg/s/MPa	u_β	Specific internal energy in phase β, J/kg
L_{inj}	Injected section length, m	α	Fracture permeability anisotropy
M	Mass or energy per volume, kg/m^3 or J/m^3	Φ	Porosity
P_f	Fracture permeability, m^2	φ	Sensitivity
P_{inj}	Bottom-hole pressure of injection well, MPa	κ	Mass components
P_r	Matrix permeability, m^2	η	Coefficient of performance
q_{inj}	Injection rate, kg/s	η_e	Conversion efficiency
R	Range	η_P	Pump efficiency
S_f	Fracture spacing, m	λ_r	Heat conductivity, W/(m·K)
S_β	Saturation of phase β	ρ_R	Rock density, kg/m^3
T	Temperature, °C	ρ_β	Density of phase β, kg/m^3
T_{pro}	Production water temperature, °C	v_β	Darcy velocity in phase β, m/s
V_n	Subdomain of the flow system	μ_β	Dynamic coefficient of viscosity, Pa·s
W_e	Power generation, MW	σ_H	Maximum horizontal stress, MPa
W_p	Pump power, MW	σ_V	Vertical principal stress, MPa
z	Depth, m	σ_h	Minimum horizontal stress, MPa

References

1. Tester, J.; Livesay, B.; Anderson, B.; Moore, M.; Bathchelor, A.; Nichols, K.; Blackwell, D.; Petty, S.; DiPippo, D.; Toksoz, M.; et al. *The Future of Geothermal Energy: Impact of Enhanced Geothermal Systems (EGS) on the United States in the 21st Century*; An Assessment by an MIT-Led Interdisciplinary Panel; Massachusetts Institute of Technology: Cambridge, MA, USA, 2006.
2. Li, S.; Wang, S.; Tang, H. Stimulation mechanism and design of enhanced geothermal systems: A comprehensive review. *Renew. Sustain. Energy Rev.* **2022**, *155*, 111914. [CrossRef]
3. Wang, J.; Hu, S.; Pang, Z.; He, L.; Zhao, P.; Zhu, C.; Rao, S.; Tang, X.; Kong, Y.; Luo, L.; et al. Estimate of geothermal resources potential for hot dry rock in the continental area of China. *Sci. Technol. Rev.* **2012**, *30*, 25–31. (In Chinese)
4. Zhang, Y.; Zhang, Y.J.; Zhou, L.; Lei, Z.H.; Guo, L.L.; Zhou, J. Reservoir stimulation design and evaluation of heat exploitation of a two-horizontal-well enhanced geothermal system (EGS) in the Zhacang geothermal field, Northwest China. *Renew. Energy* **2022**, *183*, 330–350. [CrossRef]
5. Hofmann, H.; Babadagli, T.; Zimmermann, G. Hot water generation for oil sands processing from enhanced geothermal systems: Process simulation for different hydraulic fracturing scenarios. *Appl. Energy* **2016**, *113*, 524–547. [CrossRef]
6. Barenblatt, G.; Zheltov, I.; Kochina, I. Basic concepts in the theory of seepage of homogeneous liquids in fissured rocks. *J. Appl. Math. Mech.* **1960**, *24*, 1286–1303. [CrossRef]
7. Warren, J.E.; Root, J.P. The Behavior of Naturally Fractured Reservoirs. *Soc. Pet. Eng. J.* **1963**, *228*, 245–255. [CrossRef]
8. Zeng, Y.; Su, C.Z.; Wu, N.Y. Numerical simulation of heat production potential from hot dry rock by water circulating through two horizontal wells at Desert Peak geothermal field. *Energy* **2013**, *10*, 92–107. [CrossRef]
9. Suzuki, A.; Fomin, S.A.; Chugunov, V.A.; Niibori, Y.; Hashida, T. Fractional diffusion modeling of heat transfer in porous and fractured media. *Int. J. Heat Mass Transf.* **2016**, *103*, 611–618. [CrossRef]
10. Gong, F.; Guo, T.; Sun, W.; Li, Z.; Yang, B.; Chen, Y.; Qu, Z. Evaluation of geothermal energy extraction in Enhanced Geothermal System (EGS) with multiple fracturing horizontal wells (MFHW). *Renew. Energy* **2020**, *151*, 1339–1351. [CrossRef]
11. Zhou, D.J.; Tatomir, A.; Niemi, A.; Tang, C.F.; Sauter, M. Study on the influence of randomly distributed fracture aperture in a fracture network on heat production from an enhanced geothermal system (EGS). *Energy* **2022**, *250*, 123–781. [CrossRef]
12. Pandey, S.N.; Chaudhuri, A.; Kelkar, S. A coupled thermo-hydro-mechanical modeling of fracture aperture alteration and reservoir deformation during heat extraction from a geothermal reservoir. *Geothermics* **2017**, *65*, 17–31. [CrossRef]
13. Soltani, M.; Kashkooli, F.M.; Souri, M.; Rafiei, B.; Jabarifar, M.; Gharali, K.; Nathwani, J.S. Environmental, economic, and social impacts of geothermal energy systems. *Renew. Sustain. Energy Rev.* **2021**, *140*, 110–750. [CrossRef]

14. Guo, T.; Gong, F.; Wang, X.; Lin, Q.; Qu, Z.; Zhang, W. Performance of enhanced geothermal system (EGS) in fractured geothermal reservoirs with CO_2 as working fluid. *Appl. Eng.* **2019**, *152*, 215–230. [CrossRef]

15. Huang, W. Heat extraction performance of EGS with heterogeneous reservoir: A numerical evaluation. *Int. J. Heat Mass Transf.* **2017**, *13*, 645–657. [CrossRef]

16. Guo, B.; Fu, P.; Hao, Y.; Peters, C.A.; Carrigan, C.R. Thermal drawdown-induced flow channeling in a single fracture in EGS. *Geothermics* **2016**, *61*, 46–62. [CrossRef]

17. Asai, P.; Panja, P.; McLennan, J.; Deo, M. Effect of different flow schemes on heat recovery from Enhanced Geotherm al Systems (EGS). *Energy* **2019**, *175*, 667–676. [CrossRef]

18. Patterson, J.R.; Cardiff, M.; Feig, K.L. Optimizing geothermal production in fractured rock reservoirs under uncertainty. *Geothermics* **2020**, *88*, 101–906. [CrossRef]

19. Wu, X.T.; Li, Y.C.; Tang, C.A. Fracture spacing in horizontal well multi-perforation fracturing optimized by heat extraction. *Geothermics* **2022**, *101*, 102–376. [CrossRef]

20. Fisher, A. A mathematic examination of the methods of determining the accuracy of an observation by the mean error and by the mean square error. *Mon. Not. R Astron. Soc.* **1920**, *80*, 758–770. [CrossRef]

21. Han, Y.S.; He, J.T.; Lu, Y.T. Sensitivity of the properties of the graduated compression stocking and soft tissues on the lower limb-stocking interfacial pressure using the orthogonal simulation test. *Med. Eng. Phys.* **2021**, *95*, 84–89. [CrossRef]

22. Lin, R.; Diao, X.Y.; Ma, T.C.; Tang, S.H.; Chen, L.; Liu, D.C. Optimized microporous layer for improving polymer exchange membrane fuel cell performance using orthogonal test design. *Appl. Energy* **2019**, *254*, 113–714. [CrossRef]

23. Xie, J.X.; Wang, J.S. Performance optimization of pinnate horizontal well in geothermal energy utilization with orthogonal test. *Appl. Therm. Eng.* **2022**, *209*, 118–321. [CrossRef]

24. Yu, L.K.; Wu, X.T.; Hassan, N.S.; Wang, Y.D.; Ma, W.W.; Liu, G. Modified zipper fracturing in enhance d geothermal system reservoir and analyzed heat extraction optimization via orthogonal design. *Renew. Energy* **2020**, *161*, 373–385. [CrossRef]

25. Pruess, K.; Oldenburg, C.; Moridis, G. *TOUGH2 User's Guide, Version 2.0*; Lawrence Berkeley National Laboratory: Berkeley, CA, USA, 1999.

26. Pruess, K.; Faybishenho, B.; Bodvarsson, G.S. Alternative concepts and approaches for modeling flow and transport in thick unsaturated zones of fractured rocks. *J. Contam. Hydrol.* **1999**, *38*, 281–322. [CrossRef]

27. Wu, L.; Liu, J.; Zhou, J.; Zhang, Q.; Song, Y.; Du, S.; Tian, W. Evaluation of tar from the microwave co-pyrolysis of low-rank coal and corncob using orthogonal-test-based grey relational analysis (GRA). *J. Clean. Prod.* **2022**, *337*, 130–362. [CrossRef]

28. Gao, J.; Zhang, H.J.; Zhang, S.Q.; Chen, X.B.; Cheng, Z.P.; Jia, X.F. Three-dimensional magnetotelluric imaging of the geothermal system beneath the Gonghe Basin, Northeast Tibetan Plateau. *Geothermics* **2018**, *76*, 15–25. [CrossRef]

29. Zhang, C.; Jiang, G.; Shi, Y.; Wang, Z.; Wang, Y.; Li, S.; Jia, X.; Hu, S. Terrestrial heat flow and crustal thermal structure of the Gonghe-Guide area, northeastern Qinghai-Tibetan plateau. *Geothermics* **2018**, *72*, 182–192. [CrossRef]

30. Zhang, S.Q.; Li, X.F.; Song, J.; Wen, D.G.; Li, Z.W.; Li, D.M.; Cheng, Z.; Fu, L.; Zhang, L.; Feng, Q.; et al. Analysis on Geophysical Evidence for Existence of Partial Melting Layer in Crust and Regional Heat Source Mechanism for Hot Dry Rock Resources of Gonghe Basin. *Earth Sci.* **2021**, *46*, 1416–1436.

31. Genter, A.; Fritsch, D.; Cuenot, N.; Baumgärtner, J.; Graff, J.J. Overview of the current activities of the European EGS Soultz project: From exploration to electricity production. In Proceedings of the Thirty-Fourth Workshop on Geothermal Reservoir Engineering Stanford University, Stanford, CA, USA, 9–11 February 2009. SGP-TR-187.

32. U.S. Department of Energy. *Geothermal Technologies Program 2013 Peer Review*; U.S. Department of Energy: Washington, DC, USA, 2013.

33. Lei, Z.H.; Zhang, Y.J. Investigation on the effect of symmetrical multi-well layout on geothermal energy extraction from a fractured granitic reservoir: A case study in the Gonghe Basin, Northwestern China. *Energy Rep.* **2021**, *7*, 7741–7758. [CrossRef]

34. Huang, X.X.; Zhu, J.L.; Niu, C.K.; Li, J.; Hu, X.; Jin, X.P. Heat extraction and power production forecast of a prospective enhanced geothermal system site in Songliao Basin. *China Energy* **2014**, *75*, 360–370. [CrossRef]

35. Zhang, Y.J.; Li, Z.W.; Yu, Z.W.; Guo, L.L.; Jin, X.P.; Xu, T.F. Evaluation of developing an enhanced geothermal heating system in northeast China: Field hydraulic stimulation and heat production forecast. *Energy Build.* **2015**, *88*, 1–14. [CrossRef]

36. Zoback, M.D. *Reservoir Geomechanics*, 1st ed.; Cambridge University Press: Cambridge, UK; New York, NY, USA, 2007; p. 464.

37. Hofmann, H.; Weides, S.; Babadagli, T.; Zimmermann, G.; Moeck, I.; Majorowicz, J.; Unsworth, M. Potential for enhanced geothermal systems in Alberta, Canada. *Energy* **2014**, *69*, 578–591. [CrossRef]

38. Garg, S.K.; Combs, J. A reformulation of USGS volumetric "heat in place" resource heat in place" resource estimation method. *Geothermics* **2015**, *55*, 150–158. [CrossRef]

39. NIST. Thermophysical Properties of Fluid Systems. 2010. Available online: http://webbook.nist.gov/chemistry/fluid/ (accessed on 1 January 2022).

40. Guo, L.L.; Zhang, Y.B.; Zhang, Y.J.; Yu, Z.W.; Zhang, J.N. Experimental investigation of granite properties under different temperatures and pressures and numerical analysis of damage effect in enhanced geothermal system. *Renew. Energy* **2018**, *126*, 107–125. [CrossRef]

41. Li, Z.W.; Feng, X.T.; Zhang, Y.J.; Xu, T.F. Feasibility study of developing a geothermal heating system in naturally fractured formations: Reservoir hydraulic properties determination and heat production forecast. *Geothermics* **2018**, *73*, 1–15. [CrossRef]

42. Cheng, W.L.; Wang, C.L.; Nian, Y.L.; Han, B.B.; Liu, J. Analysis of influencing factors of heat extraction from enhanced geothermal systems considering water losses. *Energy* **2016**, *115*, 274–288. [CrossRef]
43. Sanyal, S.K.; Butler, S.J. An analysis of power generation prospects from enhanced geothermal systems. In Proceedings of theWorld Geothermal Congress, Antalya, Turkey, 24–29 April 2005; pp. 1–6.